
Analysis of Structures at High Temperature

V. Thompson

CULHAM LIBRARY
REFERENCE ONLY

CULHAM LABORATORY
LIBRARY
12 DEC 1989
V B a R



© - UNITED KINGDOM ATOMIC ENERGY AUTHORITY - 1989
Enquiries about copyright and reproduction should be addressed to the
Librarian, UKAEA, Culham Laboratory, Abingdon, Oxon. OX14 3DB,
England.

Analysis of Structures at High Temperature

Vaughan Thompson

UKAEA Culham Laboratory, Abingdon, Oxon. OX14 3DB, England.

ABSTRACT

A possible consequence of a severe accident in a nuclear reactor is the raising of the temperature of structural components beyond their design range. This report reviews the methods for predicting the response of structures at high temperature with particular reference to the steel structures of PWRs and LMFBRs. The fundamental aspects of these methods are equilibrium, strain/displacement relationships and material constitutive laws. Of particular interest here is the effect of temperature on time dependent deformation under stress (creep) and on time independent plastic deformation (yielding). The analysis methods available fall into three categories, viz empirical, analytic and numerical.

The empirical method normally involves reducing the three variables stress, time and temperature to two and is often used in design basis calculations where its limitations can be accommodated with large safety factors. Methods of partly overcoming these limitations have been considered here and this approach offers a useful first step in assessing the high temperature response of structures.

For simple structures the analytical method gives workable solutions and all the important phenomena can be included, i.e. temperature dependent yielding and ductile and brittle creep. Analytical solutions have been derived here for homogeneously stressed structures (eg a thin sphere under internal pressure) for general temperature and load excursions. However the analytical methods become cumbersome for more complex structures.

Finite element, finite difference and boundary element numerical methods are commercially available and the former in particular can be applied to a very wide range of structural problems including those likely to be encountered in a severe accident. These methods do however involve large computer codes which have some limitations and it is questionable whether their potential modelling accuracy would be justified here.

The structural materials in LMFBRs and PWRs are mainly austenitic stainless steels and low alloy ferritic steels. Data for these have been gathered in generic forms and parameters derived for use in simple constitutive laws.

September 1989

CONTENTS

1. Introduction
2. General aspects of high temperature failure of steel structures.
 - 2.1 Introduction
 - 2.2 Creep
 - 2.3 Deformation mechanism maps.
 - 2.4 Types of failure at high temperature
 - 2.5 Applications to this study
3. Modelling of structures incorporating high temperature behaviour.
 - 3.1 General features
 - 3.2 Empirical approaches
 - 3.3 Analytical models
 - 3.3.1 Introduction
 - 3.3.2 Bars
 - 3.3.3 Beams
 - 3.3.4 Geometrically non-linear cases
 - 3.3.5 Axisymmetric solids
 - 3.3.6 Plates and shells
 - 3.4 Numerical methods
4. Materials data
 - 4.1 Materials involved
 - 4.2 High temperature properties
5. Recommendations
6. References

Table 1

Figures 1-12

Appendix 1 Failure of homogeneously stressed structures at high temperature

1. INTRODUCTION

This review has been done within the General Nuclear Safety of Reactors (GNSR) Programme to provide background information to help in the study of hypothetical severe accidents involving nuclear reactors (beyond design basis accidents). In particular the review has addressed the problem of determining the response of steel structures in PWRs and LMFBRs operating at temperatures above that for which they were designed due to, for example, relocation of molten fuel following a core failure. To predict the course of such an accident requires structural models which are realistic rather than conservative and are simple enough to be included with other models to represent the whole accident progression. It is anticipated that such modelling will require considerable simplification of the structure, the loads and the temperature profiles. Thus methods of estimating the errors introduced will be assessed. Structures consisting of pressure vessels under internal pressure, plates loaded out of plane, hollow cylinders loaded radially and axially, and simple frameworks will be considered as representative of reactor internal and boundary structures. This presentation of the review has been divided into these four sections:-

- (a) A general examination of the features of high temperature response of relevant materials and the types of failure mode to be expected (section 2).
- (b) A review of methods of modelling structures at high temperatures including an assessment of any model limitations (section 3).
- (c) An assessment of the available materials data for these models. Since it is likely that data will be scarce in the beyond design basis region of interest here methods of data extrapolation will be assessed (section 4).
- (d) A recommendation of the models most suitable for use in severe accident studies (section 5).

2. GENERAL ASPECTS OF THE HIGH TEMPERATURE BEHAVIOUR OF STEEL STRUCTURES

2.1 Introduction

At all temperatures all materials will fail in a time independent fashion if the applied stresses are high enough. In steels the failure mechanism can be either brittle fracture or ductile yielding. In the former little or no plastic deformation precedes failure which takes the form of a crack propagating across the structure. Ductile yielding however involves significant pre-failure plastic deformation and structural failures of this type are characterised by large permanent distortion such as plastic hinges in bending components or necking of tensile stressed components. The dominant mode depends on :-

- (a) The material and its condition e.g. extensive cold working and exposure to neutron radiation promote brittle behaviour.
- (b) The temperature - low temperatures promote brittle behaviour.
- (c) The rate of straining - high rates promote brittle behaviour.
- (d) The size of the structural sections and the defects present in them. Structures with thick sections which contain large defects are susceptible to brittle fracture.

Brittle fracture tends to be more serious as it results in abrupt failure of structures with little or no warning and is normally avoided by either:-

- (a) ensuring that if brittle failure is dominant then a large safety margin on failure exists (e.g. by keeping stresses low) or
- (b) ensuring that ductile failure dominates.

The nuclear structures in PWRs and LMFBRs are designed on the basis of (b) [1] which has the advantage over (a) in that even in the event of an unforeseen overload brittle failure is avoided.

Note that this type of low temperature brittle failure is distinct from the brittle creep failures which occur at high temperature and which will be

described below. Both forms occur at small strain but the former is transgranular, giving a smooth fracture surface whereas the latter is intergranular and has a 'frosty' fracture surface. In this report brittle failure will refer to the high temperature form unless stated otherwise.

It seems reasonable in this work that low temperature brittle fracture will be avoided since we are concerned with accidents which result in an increase in the structure's temperature which reinforces the ductile dominance. A possible exception to this, not considered here, is explosive loading which could possibly promote low temperature brittle failure by increasing the rates of straining. Time independent deformation and failure of materials can be illustrated by means of a plot of strain versus stress at constant temperature (figure 1(a)).

2.2 Creep

For absolute temperatures above about $0.3 T_m$, where T_m is the absolute melting temperature, metals subject to stress display time dependent deformation known as creep. If the stress is sustained creep results in the failure after a finite life of structures that are operating at high temperature. There are a variety of creep mechanisms and the dominant ones will depend on the stress and the operating environment as well as the material and its temperature. Creep induced deformation and failure of materials is normally illustrated by a plot of strain, ϵ , against time, t , at constant load and temperature (figure 1(b)). Three stages in the deformation are usually observed. In the primary stage, or stage I, $\epsilon \sim t^n$ where $n < 1$ and the deformation process is similar to yielding where dislocation movement allows plasticity to take place. This stage is often ignored in analyses or simply replaced by an initial value of strain. In the secondary stage, or stage II, a dynamic equilibrium between thermally induced softening and strain induced hardening is reached and $\epsilon \sim t^1$. This stage is also known as the minimum creep strain rate stage. Failure may occur at the end of stage II or after a subsequent stage III, or the tertiary stage, in which $\epsilon \sim t^n$ where $n > 1$. The transition from stage II to III may be due to structural changes due to thinning of the creep specimen or metallurgical changes due to high temperature ageing. The failure mode can be ductile or brittle according to whether the governing mechanism in stage II is power law creep or diffusional flow creep respectively [2].

Power law creep

This is so-called because the stress dependence of the strain rate is given by $\dot{\epsilon} \propto \sigma^n$ where σ is the stress and n a constant. It is due to thermal activation which permits dislocations to climb over obstacles which would be insurmountable at low temperature.

In some materials (e.g. low alloy steels) this type of creep has two forms. In the high temperature form the thermal activation is dominated by lattice diffusion. In the low temperature form diffusion of dislocation cores becomes dominant. The two forms result in different stress dependence of the strain rate i.e. $\dot{\epsilon} \propto \sigma^{n+2}$ in the high temperature regime and $\dot{\epsilon} \propto \sigma^n$ in the low temperature regime and hence the boundary between these regimes [2] depends on stress as well as temperature. It is notable that in high alloy steels, such as austenitic stainless steels, only the high temperature form occurs as the alloying components appear to resist movement of the dislocation cores.

Diffusional flow creep

This type of creep is due to movement occurring at grain boundaries due to diffusion of matter around or through these regions. Again two regimes are possible and are characterised by temperature. The high temperature form is due to lattice diffusion and is also known as Nabarro-Herring creep. In the low temperature form grain boundary diffusion dominates and this is also known as Coble creep. Both regions of diffusional flow creep are characterised by a linear dependence of strain rate on stress i.e. $\dot{\epsilon} \propto \sigma^1$, at constant temperature, and only dominates over the power-law creep when the stresses are low.

2.3 Deformation mechanism maps

The various mechanisms described above can be conveniently illustrated using these maps. Figure 2 from data in [2] shows maps for stainless steel type 316 and pure iron. These materials are representative of the austenitic stainless and the ferritic low alloy steels used in PWRs and LMFBRs. The maps indicate the dominant deformation modes for the materials at constant stress and temperature in the virgin state. The ordinate σ_s/μ is the shear stress normalised to the shear modulus and the abscissa

is the absolute temperature normalised to the absolute melting temperature (T/T_m). Contours of constant strain rate are indicated. On the stainless steel map regions representing (a) the raw creep data used in constructing the maps, and typical operating regimes for LMFBR components for (b) design basis conditions and (c) possible severe accident conditions. It is interesting to note the extrapolations from the raw data necessary to cover both design and beyond design basis regions. In particular for this study we are interested in the response of materials up to melting but the raw data exists only for typically $T < 0.65 T_m$. There is however some raw data given in [2] for pure iron up to $0.9 T_m$ which supports the basis of the extrapolations used in constructing the maps at least to this point.

These maps can be used to estimate the variation of yield stress with temperature providing the variation of the shear modulus, μ , or alternatively the variation of Young's modulus with temperature is known. Young's modulus falls steeply with temperature as the melting point is approached and the actual value at melting is sensitive to the extrapolation used. Moreover the extrapolations cannot be checked since there are no data beyond $T = 0.9 T_m$. This is an important point here since the failure mode - melting versus yielding - may be sensitive to the modelling and if this is the case reliable results cannot be obtained. The uncertainty in the value of Young's modulus at melting can be gauged from the data given in [2] and [3]. From [2] these values divided by the room temperature value are $\sim 35\%$ for stainless steel and 13% for low alloy steels. From figure 3 based on data in [3] the corresponding figure is $\lesssim 5\%$ in both cases.

It may seem at first sight that the materials data base could be usefully extended to avoid extrapolations into the high temperature region. However the impracticality of performing the necessary measurements can be demonstrated by considering the measurement of say the yield stress of 304 stainless steel at 1000°C ($0.75 T_m$). This would require an applied stress of some 50 MN/m^2 which would result in creep deformation of $\sim 1\%$ /minute at this temperature which would swamp the measurements of yield deformation. Measurement of the Young's modulus is somewhat more practical however at these high temperatures since it can be inferred from velocity of propagation of elastic waves. It is interesting to note that extrapolations into the design basis region are also commonly required but for the opposite reason i.e. design basis creep rates are likely to be so small (typically

less than 1% strain in 30 years) that measurements over practical test timescales are not possible.

2.4 Types of Failure at High Temperature

The maps of deformation processes described above can be supplemented by maps which give details of failure modes. Fracture-mechanism maps [4 and 5] use the same axes as before and indicate failure modes of specimens tested assuming that load and temperature remain fixed throughout the test. Figure 4(a) is a map for 304 stainless steel from data in [4] and is qualitatively typical of austenitic stainless steels. Contours of constant time to failure (c.f. contours of constant strain rate on the deformation maps) are shown. An alternative form of the map is reproduced in figure 4(b) where the normalised stress is plotted against time with isotherm contours. Note that the boundaries between failure modes are not always abrupt and in some cases mixed failure modes can occur.

These maps exhibit many features of the deformation maps but give important additional information due to the results representing the whole specimen life rather than the initial deformation excursion. In particular dramatic changes in cross-section occur prior to failure in some regions and long term changes in micro-structure sometimes occur due to prolonged exposure at high temperature. Both of these effects are absent in the deformation maps. The failure modes relevant to stainless steel and other face centered cubic (f.c.c.) metals are ductile fracture, trans-granular creep fracture, inter-granular creep fracture and rupture.

Ductile Fracture

This corresponds to the yielding region in the deformation maps which starts with deformation due to dislocation glide and proceeds by voids nucleating at inclusions which then elongate and finally link as the intervoid connections shrink due to the specimen necking. In the case of cylindrical specimens the voids link into sheets which give the characteristic cup-and-cone fracture surface. This surface is fibrous and trans-granular.

Trans-granular Creep Fracture

This mechanism is initiated by creep deformation when $T \gtrsim 0.3 T_m$ and progresses through void nucleation and growth in a similar way to ductile fracture. There are differences however due to (a) stress levels being generally lower which may delay nucleation and (b) diffusion which may influence void growth. However the fracture surface and ductility are similar.

Inter-granular Creep Fracture

At lower stresses and higher temperatures the creep mechanism is dominated by diffusional flow at grain boundaries and this leads to growth of voids there which ultimately link causing inter-granular fracture. This failure mode is characterised by low ductility (i.e. very little specimen necking) and long times to failure compared with trans-granular creep fracture.

Rupture

This occurs when necking is able to progress until the specimen cross-section has shrunk to virtually zero. It really represents a structural (i.e. specimen dependent) rather than a material failure and occurs when all other modes are prevented due to suppression of either void nucleation or void growth. It commonly occurs in f.c.c. metals at high stress and high temperature which allow dynamic recrystallisation to occur and this suppresses nucleation. This process occurs during forging. It also occurs at high temperatures if dissolution of precipitates, such as carbides in 304 stainless steel at $T > 0.75T_m$, removes the void nucleation sites.

2.5 Applications to this study.

These maps can be very useful aids to understanding the behaviour of structures at high temperature but the following restrictions should be noted:-

(a) The deformation maps give information only about the initial deformation changes for material in its virgin state.

(b) The maps generally relate to constant load, constant temperature tests on uniaxially stressed tensile cylindrical specimens since these are used to generate the bulk of creep data.

The effects of variations in temperature and stress experienced by real structures can however be accommodated by using a cumulative damage law. This states that failure will occur when:-

$$\int_0^{t_f} dt/t_f(\sigma, T) = 1 \quad (2.1)$$

where $t_f(\sigma, T)$ is the failure time measured in a constant stress σ , constant temperature T , test but is assumed to hold for cases where σ and T vary within a single test ([6] and [7]). Note that normally in creep tests the load is kept constant and the stress increases as the specimen necks, but as this occurs towards the end of the specimen life the effect on t_f is minimal. This law is derived from the assumption that the rate of change of some parameter which characterises damage, e.g. strain, depends only on time through the variation of stress and temperature i.e.:-

$$\dot{\epsilon} = f(\sigma(t), T(t)) \quad (2.2)$$

and $\epsilon(\text{fail}) = \text{constant} \quad (2.3)$

Integrating this from $\epsilon = 0$ to $\epsilon(\text{fail})$ and putting $t_f(\sigma, T) = \epsilon(\text{fail})/f(\sigma, T)$ gives (2.1). Robinson [8] discusses this assumption and gives some evidence of support from experiments on steels but note the following restrictions:-

(a) If the excursions of stress or temperature cross a mechanism boundary the form of the damage will change and the law will be invalidated, although clearly if the damage in all regions except one is minimal the error will be small.

(b) The form of equation (2.2) changes if unloading takes place and so the law cannot be used in the form above if stress or temperature varies cyclically (fatigue loading). This should not affect the present study however since a severe accident would normally result in monotonic variations and failure would occur, if at all, before unloading started.

The law can also be used to extrapolate creep data to high temperatures provided the form of $f(\sigma, T)$ or $t_f(\sigma, T)$ for the whole of a region can be determined from tests in one part and the extrapolation does not cross a mechanism boundary. The Dorn form of the creep strain variation with temperature [9] provides a convenient and commonly used way of doing this:-

$$\dot{\epsilon} \sim \exp(-Q/RT) \quad (2.4)$$

where Q is the activation energy and R the universal gas constant. The constant of proportionality and possibly Q will vary with stress but this variation can be determined at manageable temperatures.

Effect of test specimen

The maps are based on cylindrical specimen tests which have uniaxial and homogeneous (up to necking) stress systems and in general cannot be rigorously applied to other structures. In particular:-

(a) Deformation geometry influences the relation between deformation and stress. In some structures the stresses reduce initially as deformation proceeds (e.g. a flat plate loaded out of plane) whereas in the tensile creep test the stresses are independent of deformation until necking.

(b) Inhomogeneous stress systems can result in a different type of failure mode. For example a ductile beam loaded in bending cannot fail by necking - it merely distorts into a tight curve or hinge.

(c) Multiaxial stress systems (e.g. a sphere under internal pressure) influence the behaviour but these can be related to uniaxial tests. This will be described in section 3.

Thus in all but the simplest cases the interpretation of creep tests to real structural behaviour involves a separate analysis which has three stages. Firstly a constitutive law which allows strains to be computed from stresses and any other relevant parameter must be deduced from the tests. Secondly the appropriate failure criteria must be developed and finally these must be incorporated into a model of the structural behaviour. There are many ways of applying these stages and these will be described in detail below. However even at this stage two very important

conclusions can be drawn from the creep data for steels and the associated maps which are pertinent to the present study:-

(a) A severe accident which increases the structure temperature will make ductile failure more likely even if the stresses also increase.

(b) A critical time exists below which brittle creep failure cannot occur at any temperature or stress and this failure mode can thus be excluded from studies of brief events. This time is ~ 5 hours for 304 stainless steel and ~ 15 hours for pure iron.

3. MODELLING OF STRUCTURES INCORPORATING HIGH TEMPERATURE BEHAVIOUR

3.1 General features.

Any analysis to determine the response of a structure to applied loads involves four stages:-

(a) Equilibrium. For static or quasi-static responses of structures the internal stresses, σ_{ij} , must be in equilibrium with any internal body forces, f_i , and any surface tractions. In cartesian co-ordinates, x_i , these are given by three equations [10]:-

$$\frac{\partial \sigma_{ij}}{\partial x_j} + f_i = 0 \quad (3.1)$$

(b) Strain displacement relations. For homogeneous displacements u_i of a continuum there exists a strain tensor, ϵ_{ij} , which characterises the state of deformation of real solids and is related to the displacements through [10]:-

$$\epsilon_{ij} = \frac{1}{2} \left(\frac{\partial u_i}{\partial x_j} + \frac{\partial u_j}{\partial x_i} \right) + \frac{1}{2} \frac{\partial u_k}{\partial x_i} \frac{\partial u_k}{\partial x_j} \quad (3.2)$$

Note that ϵ_{ij} is independent of the rigid body components of displacement and that the off-diagonal terms used in [10] have been multiplied by $\frac{1}{2}$ to make ϵ_{ij} a tensor. Equation (3.2) is valid for arbitrarily large displacements in Lagrangian co-ordinates but the displacements themselves cannot be arbitrary - they must satisfy continuity. A small displacement approximation is given by dropping the second order terms. The strain tensor must satisfy the following compatibility conditions [10]:-

$$\frac{\partial^2 \epsilon_{22}}{\partial x_3^2} + \frac{\partial^2 \epsilon_{33}}{\partial x_2^2} = 2 \frac{\partial^2 \epsilon_{23}}{\partial x_2 \partial x_3} \quad ; \quad \frac{\partial^2 \epsilon_{11}}{\partial x_2 \partial x_3} = \frac{\partial}{\partial x_1} \left(\frac{\partial \epsilon_{31}}{\partial x_2} + \frac{\partial \epsilon_{12}}{\partial x_3} - \frac{\partial \epsilon_{23}}{\partial x_1} \right) \text{ etc.} \quad (3.3)$$

Note there are other definitions of large displacement strain such as the natural (or logarithmic) strain which will be used in sections 3.2, 3.3 and the appendix.

(c) Constitutive law. This relates stress to strain and any other relevant parameters e.g. strain rate, $\dot{\epsilon}$, temperature, T , and time, t . In

the case of uniaxial stress this can usually be expressed by a function which in principle can be determined from uniaxial stress tests:-

$$\epsilon = f(\sigma, \dot{\epsilon}, T, t, \text{ etc.}) \quad (3.4)$$

In some cases, e.g. creep recovery, the strain may depend on the history of the previous loading and the function $f(\dots)$ will then involve a convolution integral. Also the form of $f(\dots)$ will in some cases depend on whether the material is being loaded or unloaded.

When multi-axial stress systems are encountered it is not practical to extend the function $f(\dots)$ to cover all possibilities so theories have been developed to relate multi-axial constitutive laws to uniaxial tests.

Multi-axial constitutive laws

The simplest constitutive law is based on linear elastic behaviour which characterises many materials deforming at low temperatures with small strains. This is known as Hooke's law:-

$$\sigma_{ij} = D_{ijkl} (\epsilon_{kl} - \alpha_{kl} \Delta T) \quad (3.5)$$

where D_{ijkl} is the matrix of elastic constants and α_{ij} are the expansion coefficients. These can be made temperature dependent if necessary. In severe accidents however we are concerned with materials that do not obey Hooke's law because at high temperature materials become weaker, the elastic limit may be exceeded and time dependent deformations may occur. I.e. we must consider plasticity and creep.

The constitutive law for non-elastic behaviour was originally formulated for the case of pure plasticity but the same derivation has subsequently been applied to combined plasticity and creep (see for example [11]). The law stems from Druker's postulate - "the work of any additional action on the displacement that it produces is non-negative for a closed cycle". Although similar to, this is not related to, the laws of thermo-dynamics. In effect it asserts the existence of materials which are stable when loaded and dissipate energy when subjected to non-elastic deformation. The postulate can be expressed as:-

$$\oint (\sigma_{ij} - \sigma_{ij}^*) d\epsilon_{ij} \geq 0 \quad (3.6)$$

where σ_{ij}^* is the initial stress state. By suitable choice of integral path it can be shown that:-

$$d\sigma_{ij} d\epsilon_{ij}^n \geq 0 \quad (3.7)$$

where the strain has been separated into elastic and non-elastic components

$$\epsilon_{ij} = \epsilon_{ij}^e + \epsilon_{ij}^n \quad (3.8)$$

From these it follows that (a) the non-elastic strain increment, $d\epsilon_{ij}^n$, is normal to the surfaces $\sigma_{ij}\epsilon_{ij} = \text{constant}$, (b) these surfaces are convex and (c) that a potential Φ exists such that:-

$$d\epsilon_{ij}^n = \partial\Phi/\partial\sigma_{ij} \quad (3.9)$$

In general Φ will depend on the stress, σ_{ij} , the material properties and the other parameters which characterise the material in the uniaxial case. The potential, Φ , is related to the dissipation of energy which is a scalar and can only depend on the three scalar invariants of the stresses ($\sigma_{ii}, \sigma_{ij}\sigma_{ij}, \sigma_{ij}\sigma_{jk}\sigma_{ki}$). Normally in plasticity theory the equivalent invariants σ, σ_o, θ are used so that:-

$$\Phi = \Phi(\sigma, \sigma_o, \theta) \quad (3.10)$$

$$\sigma = \frac{1}{3} \sigma_{ii} \quad (3.11)$$

$$\sigma_o^2 = \frac{3}{2} \sigma_{ij} \sigma_{ij} - \frac{1}{2} \sigma_{ii} \sigma_{jj} = \frac{3}{2} \sigma_{ij}' \sigma_{ij}' \quad (3.12)$$

$$\sigma_i = \sigma + \frac{2}{3} \sigma_o \cos \left[\theta - \frac{2(i-1)\pi}{3} \right] \quad (3.13)$$

Here σ_{ij}' is the stress deviator $\sigma_{ij} - \frac{1}{3} \delta_{ij} \sigma_{kk}$ (δ_{ij} is the kronecker delta tensor) and σ_i are the principal stress components. Physically σ is the mean or hydrostatic stress, σ_o is proportional to the maximum shear

stress on the octahedral plane (ie the plane making equal angles with axes parallel to the principal stress directions, figure 5(a)) and θ is the angle in this plane between the direction parallel to the maximum shear stress and the intersection with the 1 axis. It is commonly observed in metals that non-elastic deformation is incompressible which implies that the dependence of Φ on σ can be ignored and that the $\Phi = \text{constant}$ surfaces in principal stress space are co-axial with the line $\sigma_1 = \sigma_2 = \sigma_3$ and can thus be conveniently plotted on a plane perpendicular to this line (π plane). See figure 5(b).

Two main theories have been developed to account for the dependence on the remaining two invariants and in both cases these have been reduced to a single scalar on the basis of experimental observation [11].

In the Von Mises theory $\Phi = \Phi(\sigma_o)$ and the $\Phi = \text{constant}$ surfaces are circular cylinders perpendicular to the π plane and intersect the σ_1, σ_2 plane in an ellipse. In the St. Venant theory (or Tresca theory for the purely plastic case) $\Phi = \Phi(\sigma_o g(\theta))$ where:-

$$g(\theta) = \frac{2}{\sqrt{3}} \cos \left(\theta - \frac{\pi}{2} \right) \quad \frac{\pi}{3} \leq \theta \leq \frac{2\pi}{3} \text{ etc.} \quad (3.14)$$

Here the $\Phi = \text{constant}$ surfaces are regular hexagonal prisms which intersect the σ_1, σ_2 plane in an irregular hexagon (figure 5(c)).

The theories are based on the premise that the magnitude of the non-elastic deformation is governed solely by either the shear strain energy density (Von Mises) or the maximum shear stress (Tresca). A review of experimental evidence in [11] indicates that the Von Mises theory is slightly more accurate but the difference between the two is small and any errors in either case are likely to be small in comparison with others in the analysis of real structures. The choice between them is thus normally based on ease of application. In this work the Von Mises theory will be used unless stated.

The uniaxial deformation can now be related to the multi-axial case using the Von Mises theory:-

$$d\epsilon_{ij}^n = \frac{1}{2\sigma_0} \frac{d\Phi}{d\sigma_0} (3\sigma_{ij} - \delta_{ij} \sigma_{kk}) \quad (3.15)$$

$$\text{where } \frac{d\Phi}{d\sigma_0} = \sqrt{\left(\frac{2}{3} d\epsilon_{ij}^n d\epsilon_{ij}^n\right)} \equiv d\epsilon_0$$

These are known as the Prandtl-Reuss flow equations. In the uniaxial test $\sigma_0 = \sigma_1$, and the significant strain increment, $d\epsilon_0 = \frac{2}{3} d\epsilon_{11}$, so that measurements of ϵ_1 and σ_1 under the appropriate conditions give the required data.

(d) Failure criteria

The stages above define the structural problem in sufficient detail for solutions to be obtained, at least in principle. In the cases of interest here these solutions will be in the form of time variations of displacements, strain and stress. It remains to decide when failure is deemed to occur. At high temperature this is most likely to be due to a ductile instability or brittle creep as described in section 2. The onset of a ductile instability can be found from the solutions by the condition $\dot{\epsilon}$ or $\dot{\sigma} \rightarrow \infty$ and this has been demonstrated in the examples in the appendix. There will be a stage beyond this condition in which the structure actually fails by rupture or ductile fracture but this normally occurs very quickly after the instability starts and no attempt has been made to model this here. The onset of brittle creep failure must be examined by other criteria. One method uses a damage parameter (Kachanov method) and will be described in detail in section 3.3.2.

3.2 Empirical approaches

It is clear from the above that analysis of even moderately complicated structures at high temperatures is likely to be very involved. Also the material data available to the analyst is likely to be associated with short time tests which may need to be extrapolated for design basis studies to service conditions lasting many years. For these reasons, approximate methods of estimating the response of creeping structures have been proposed. These are based partly on theory and partly on experimental observations and provide very useful tools for obtaining rapid estimates of

structure performance. For design basis calculations these are often the only methods used since the errors associated with the approximations can usually be accommodated by use of conservative design safety factors. However even for severe accident studies these methods are also of interest if only as a preliminary to a more involved analysis.

The methods involve reducing the three primary independent variables (viz. time, temperature and stress) to two so that certain creep conditions e.g. creep rupture, can be presented on a single graph. The raw data for the methods are normally based on creep tests performed at constant temperature and constant load. The validity of the subsequent extrapolations to structures in which the temperature and load may vary are discussed below. There are three basic assumptions to the methods:-

(1) There are two types of independent creep deformation and failure viz. ductile or brittle.

(2) A simple analytical form of the constitutive law for the creep strain for each type of deformation exists. i.e.

$$\dot{\epsilon}_c = g(\sigma, T, t) \quad \text{where } g(..) \text{ is of known form.} \quad (3.16)$$

(3) The product of secondary stage creep rate and time to failure is approximately constant independent of stress and temperature, i.e.:-

$$\dot{\epsilon}_c t_f \approx \text{constant} = \epsilon^* \text{ say} \quad (3.17)$$

The third assumption is based on experimental observations but also has a theoretical basis and is illustrated in figure 6(a). It implies that the strain at the end of the secondary stage of creep where the strain rate is approximately constant depends only on whether the deformation is ductile or brittle. A simple theoretical basis for this in the ductile regime at constant temperature was demonstrated by Hoff using a simple power law form of the creep law and ignoring plastic deformations (e.g. [6]), i.e.:-

$$\dot{\epsilon}_c = B \sigma^n \quad (3.18)$$

where B and n are constants. The time to failure, t_f , is given by:-

$$t_f = \int_{\epsilon_0}^{\epsilon_f} d\epsilon / (B\sigma^n) \quad (3.19)$$

For a round bar in tension undergoing constant volume deformation and using the natural strain formulation gives $d\epsilon = dl/l = -dA/A$ where A is the cross-sectional area and l the length of the bar. Thus:-

$$t_f = - \int_{A_0}^{A_f} A^{n-1} dA / (B P^n) \quad (3.20)$$

where P is the tensile load on the bar and is assumed constant. A_0 and A_f are the initial and final cross-sectional areas respectively. If purely ductile failure occurs then $A_f \ll A_0$ and thus:-

$$t_f = (A_0/P)^n / (nB) = (n\dot{\epsilon}(t=0))^{-1} \quad (3.21)$$

This corresponds with (3.17).

When the failure is brittle the strain at failure is governed by the accumulation of deformation at grain boundaries which precipitates failure when these boundaries have deformed by an amount dependent only on the grain size [12]. Hence for a given material and grain size the strain at failure is constant, and since the strain rate will be approximately constant at constant stress and temperature in the non-ductile regime, (3.17) follows directly. Note however that the creep strain at failure is not always constant since the secondary stage in the ductile regime will be followed by a third stage in which the strain rises steeply. A plot of creep strain to failure versus failure time for steels would normally be as shown in figure 6(b).

The form of the function $g(\cdot)$ determines the method and more than 20 have been proposed [12]. Some of these have been examined in [11] and details of four are given below.

Larson-Miller. This is the most commonly used correlation and is based on:-

$$\dot{\epsilon}_c = A \exp \left(\frac{B\sigma - Q}{RT} \right) \quad (3.22)$$

where A, B and Q are material constants. From (3.17) and (3.22) it follows that:-

$$T [C + \log(t_f)] = p = F(\sigma) \quad (3.23)$$

where C is a constant, t_f is conventionally measured in hours and $F(\sigma)$ is a linear function of σ . p is known as the Larson-Miller parameter and by suitable choice of the constant C can be used to characterise creep failure of many metals by plotting p against σ or $\log(\sigma)$. C for steels is in the range 16-24. Figure 7(a) shows a Larson-Miller plot for austenitic stainless steel from data in [13] and is typical of many steels. The two straight portions of the plot represent ductile failure (at high stress or low p) and brittle failure (at low stress or high p).

Manson-Haferd. These authors proposed a similar method to Larson and Miller's but included an additional constant to give more flexibility with the following expression:-

$$\frac{T - T_a}{\log(t_f) - \log(t_a)} = F(\sigma) \quad (3.24)$$

where T_a and t_a are constants.

Manson-Succop. This correlation is given by [12]:-

$$CT + \log(t_f) = F(\sigma) \quad (3.25)$$

C is a constant. This correlation has been examined by Clauss [14] who found it gave better results for steels than Larson-Miller. In particular Clauss noted that Larson-Miller correlations produced a small but definite systematic error since points of short life always lie above the correlation and those of long life always below it. Figure 7(b) and 7(c) from data in [14] illustrate this using data from Timken 35-15 stainless steel. This is an important point here since the Larson-Miller correlations appear unsuitable for use where large extrapolations from the raw data may be required.

Orr, Sherby and Dorn. This method is based on the Dorn form of the creep strain equation:-

$$\dot{\epsilon}_c = (\sigma/\sigma_c)^n \exp(-Q/RT) \quad (3.26)$$

where σ_c , Q and R are constants. From (3.26) and (3.17) it follows that:-

$$t_f \exp(-Q/RT) = \theta = \epsilon^* (\sigma/\sigma_c)^{-n} \quad (3.27)$$

The Dorn parameter, θ , can be plotted against σ as for the Larson-Miller case. Figure 7(d) and 7(e) from data in [11] compare Larson-Miller and Dorn correlations for stainless steel and indicates the superiority of the latter for this material.

Use of empirical methods in severe accident studies.

When applying these methods to severe accident studies the following limitations should be noted:-

- (1) The methods are usually aimed at design basis conditions and in particular the raw data used may have been obtained at only moderate temperatures. Higher temperature data may result in different constants in the correlations.
- (2) The methods of predicting failure are based on constant load tensile specimens in which the stress remains constant until either necking takes place or brittle failure occurs.

In a design basis calculation this second point would not normally be a limitation since the deformation of the real structure should be small over its design life. In a severe accident however large deformation may precede failure and the stresses may alter considerably.

This can be illustrated by considering the static ductile failure of the four types of structure shown in figure 8. The creep tension specimen is shown in figure 8(a). The axial load P increases linearly with axial deflection, u , until this becomes so large (λ specimen length) that the cross-sectional area reduces significantly and the specimen necks. P reaches a maximum value and failure follows.

The cantilevered beam in figure 8(b) shows similar behaviour initially but now the stresses change through the thickness and necking cannot occur. A

plastic hinge forms at the root of the cantilever and the structure continues to deform, without reaching a maximum load, until some other mechanism takes over, e.g. transfer of the load to another structure.

The built-in beam of figure 8(c) is also similar to case (b) for small deflections as $P \propto u$ for small u but when $D < u < L$ where D is the depth of the beam the behaviour changes. The stress system transfers from the bending case of (b) to the membrane case of (a) due to geometrical stiffening afforded by the axial constraint. For $u \ll L$ thinning of the section occurs and a maximum load is reached as in case (a).

For some structures this geometrical non-linearity can be of opposite sign such as for the Euler strut shown in figure 8(d). Here a drop in stiffness occurs at moderate deformations. This is known as buckling.

These four types of behaviour have counterparts in structures formed from plates and shells. For structures operating at high temperature these deformation stages can be traversed at constant load due to creep and ductile failure will occur at similar deformations to the static cases above. However if brittle creep is dominant failure may occur at an earlier stage.

It is thus evident that the nature of the large deformation behaviour of the structure must be considered when analysing severe accidents which from the points discussed in section 2.4 would be expected to result in ductile failure.

3.3 Analytical Models.

3.3.1 Introduction

In this section the methods available for analysing structures which exhibit creep and permit analytical solution are reviewed. By analytical solution it is intended to include methods which generate solutions requiring simple numerical methods to compute the actual results, but not methods using numerical techniques a priori. These will be covered in section 3.4. It is necessary first to categorise the analytical methods according to the type of structure being analysed, the nature of the loads and the types of solution generated. Here we consider bars, beams,

plates, shells and axisymmetric solids. From these components most practical structure can be produced. Analytical solutions for general solid structures not covered by these are very rare even without the complication of creep and with such structures only numerical methods can be used.

The next categorisation that must be established is whether the structure is statically determinate or indeterminate. This depends both on the structure and the nature of the loads. In a determinate structure (e.g. a bar in tension) the internal forces or stresses can be determined solely on the basis of equilibrium with the externally applied loads, whereas in an indeterminate structure (e.g. a beam built-in at both ends) application of equilibrium alone leaves a certain number of unknown forces (or moments) which can only be found by considering the compatibility of the structure and its supports.

A third categorisation must be made as to whether the solution which is generated will be steady state or transient. Steady state solutions are much simpler and apply to cases where the loads and the stresses are independent of time. The material must be deforming in the secondary creep regime where the creep strain increases linearly with time and thus the strain rate (and hence the stresses) are time independent. This is a somewhat restrictive class of solution but actively pursued in most texts on creep because of the simplicity of the steady state solutions. In particular structures such as plates loaded out of plane will show different behaviour for small and large deflections due to geometrical non-linearity as discussed section 3.2 and this excludes a steady state response. Also the third stage of ductile creep, where the stresses increase due to reductions in cross-sectional area, cannot be included in steady state solutions.

3.3.2 Bars

In structural terms a bar is a prismatic body loaded at its ends to produce an homogeneous stress system. Only tensile loads will be described here. Compressive loads eventually lead to distortion which destroys the stress homogeneity - this is known as creep buckling and will not be covered here although the methods described below can be extended to cover this phenomenon. A bar in tension is the simplest structure to analyse and it

is possible to include all the important effects due to creep, some of which have to be abandoned or simplified in other structures. It is necessary to assume however that the stress system remains homogeneous. Thus when necking occurs due to failure as a result of ductile creep the homogeneous solution ceases to be valid, but many important results can be obtained from the solution up to this point. In particular the combinations of load, time and temperature to failure can be predicted and the pre-necking deformation.

To illustrate this consider a material with a constitutive law given by superposition of a time independent plastic strain ϵ_p , and a time dependent creep strain ϵ_c .

$$\text{i.e.} \quad \epsilon = \epsilon_p(\sigma, T) + \epsilon_c(\sigma, T, t) \quad (3.28)$$

If the length of the specimen is x , with an initial value x_0 , then the increment in strain caused by an increase in x is given by $d\epsilon = dx/x$ (natural strain). Hence allowing for large deformation:-

$$\epsilon = \ln(x/x_0) \quad (3.29)$$

From the condition of incompressibility, the cross-sectional area A , with initial value A_0 , must satisfy:-

$$xA = x_0 A_0 \quad (3.30)$$

Hence $A = A_0 \exp(-\epsilon)$ and the true stress, σ , is given by:-

$$\sigma = \sigma_0 \exp(\epsilon) \quad (3.31)$$

where $\sigma_0 = L/A_0$ is the nominal stress, i.e. the load, L divided by the initial cross-sectional area. Hence if the temperature, T , is constant

$$\dot{\epsilon}_c = \dot{\sigma} \left(\frac{1}{\sigma} - \frac{\partial \epsilon_p}{\partial \sigma} \right) \quad (3.32)$$

Once the dependences of plastic strain and creep strain rate with stress are known this equation can be integrated to give the stress (or strain) variation with time:-

$$t = \int_{\sigma_0}^{\sigma} \frac{d\sigma}{\dot{\epsilon}_c \sigma} \left(1 - \sigma \frac{\partial \epsilon_p}{\partial \sigma}\right) \quad (3.33)$$

Typical solutions are illustrated in figure 9(a). The special case described by Hoff is generated by ignoring the plastic strain (i.e. $\epsilon_p = 0$) and assuming a power law for the creep strain rate i.e.

$$\dot{\epsilon}_c = B \left(\frac{\sigma}{\sigma_c}\right)^n \quad (3.34)$$

This gives a solution for the strain which tends asymptotically to infinity as t approaches t_H where:-

$$t_H = \frac{1}{nB} \left(\frac{\sigma_c}{\sigma_0}\right)^n \quad (3.35)$$

A more realistic response can be obtained by including a plastic strain term based on another power law i.e.:-

$$\epsilon = \left(\frac{\sigma}{\sigma_p}\right)^m + \int B \left(\frac{\sigma}{\sigma_c}\right)^n dt \quad (3.36)$$

This gives a solution which is illustrated by curve 1 in figure 9(a). Beyond point D the solution ceases to be valid as $\dot{\epsilon} < 0$ implies unloading and equation (3.36) is only valid while loading occurs. In fact point D represents the onset of necking because small variations in cross-sectional area will mean that this point is reached first at one particular section of the rod, the deformation then becomes unstable at this section ($\dot{\epsilon} \rightarrow \infty$) and the necking process takes over. This will occupy very little additional time and so the failure time is given closely by the time at D, t_D where:-

$$t_D = t_H \left[1 - \frac{m}{m-n} \left(\frac{\sigma_0}{\sigma_p}\right)^n + \frac{nm}{m-m} \left(\frac{\sigma_0}{\sigma_p}\right)^m\right] \quad (3.37)$$

This analysis assumes that failure is dominated by ductile creep. A means of analysing situations in which brittle creep behaviour is possible was formulated by Kachanov. The method is described in [7] and is based on the hypothesis that ductile and brittle creep occur as independent mechanisms. This is justified by the fact that brittle creep failure is due to the accumulation of internal voids at grain boundaries which at least to a

first approximation should be independent of the ductile creep process which involves movement within the grains. The mechanisms can however be linked indirectly by the applied stresses since ductile creep can cause reductions in cross-section which increases the stress, which in turn can affect the brittle response. Kachanov considered the brittle creep voids as a reduction in the load carrying area of the structure and introduced a damage factor D where :-

$$D = (A - A_r) / A \quad (3.38)$$

A is the apparent cross-sectional area, with initial value A_0 , and A_r is the reduced area representing the material remaining when the internal voids are taken into account. $D=0$ corresponds to material undamaged by brittle creep and $D=1$ corresponds to brittle creep failure. It is now necessary to model the variation of D with time and in the simplest model proposed by Kachanov this becomes:-

$$\frac{dD}{dt} = C \left(\frac{\sigma}{1-D} \right)^v \quad (3.39)$$

Note that the stress σ , is still the load divided by the apparent area which is consistent with the ductile analysis, and the term $\sigma/(1-D)$ is the load divided by the reduced area which is assumed to govern the progress of brittle creep as reflected in equation (3.39). C and v are material constants which would be determined from constant load, constant temperature creep tests performed in the brittle regime such that the change in A is negligible. In such cases the stress, σ , is constant and equation (3.39) can be integrated from $D=0$ to 1 and $t=0$ to t_B , to give:-

$$t_B = (1 + v)^{-1} C^{-1} \sigma_0^{-v} \quad (3.40)$$

The combination of brittle and ductile creep behaviour can now be modelled for the case of a bar in tension. To illustrate this here we will only consider creep strain, the fuller case where plastic strain is included gives similar results and is given in [6]. Using the results from the example above the stress variation with time in the absence of plastic deformation can be shown to be:-

$$\frac{\sigma}{\sigma_0} = \left[1 - \left(\frac{t}{t_H}\right)\right]^{-1/n} \quad (3.41)$$

Substituting this into the Kachanov equation gives:-

$$\frac{dD}{dt} = (1-D)^{-v} C \sigma_0^v \left[1 - \left(\frac{t}{t_H}\right)\right]^{-v/n} \quad (3.42)$$

Separating the variables and integrating this from $D=0$ to 1 and $t=0$ to t_{DB} where t_{DB} is the time to brittle failure taking into account ductile stress changes gives:-

$$\frac{t_{BD}}{t_H} = 1 - \left[1 - \frac{(n-v)t_B}{nt_H}\right]^{-v/n} \quad (3.43)$$

This result is valid provided brittle failure occurs before ductile failure, i.e. the failure time $t_f = t_{BD}$, provided $t_{BD} < t_H$, otherwise the failure is ductile and $t_f = t_H$. The dependence of failure time on initial stress, σ_0 is illustrated in figure 9(b). The form of this curve is commonly observed in experimental results (c.f. figure 7(a)) which normally exhibit two regimes, a ductile one at high stress with $d\sigma_0/dt_f$ small and a brittle one at low stress with $d\sigma_0/dt_f$ large. Note that for ductile failure the brittle and ductile components do not interact, the Kachanov equation serves only to establish the limit of ductile failure, but in the brittle regime the solutions interact and t_{BD} is different from the pure brittle failure time t_B although these converge asymptotically as $\sigma_0 \rightarrow 0$. This absence of interaction has also been verified experimentally by 'aging' materials to near failure in the brittle regime. The ductile failure performance of these materials, from further tests in the ductile regime, was then found to be comparable with 'unaged' stock [12].

The methods illustrated here for analysis of bars can be generalised to any structure with an homogeneous stress system such as thin walled tubes or spheres under internal pressure. It is also possible to include the effects of temperature changes in time which influences the creep and plasticity material properties. These general solutions are described in the appendix.

3.3.3. Beams

The simplest case of a structure with a non-homogeneous stress system is a beam under pure bending. When analysing beams analytically the assumption that plane sections remain plane as the beam deforms is almost invariably used. This is sometimes known as the St. Venant hypothesis. This considerably simplifies the analysis and appears to give accurate results provided the beam is thin compared with its length. This hypothesis has equivalent formulations for thin plates and thin-walled shells.

The simplest creep solution that can be obtained for a beam is the steady state statically determinate solution. In this case the bending moment in the beam is a known function of position (i.e. $M=M(x)$) and the stresses in the beam are a time independent function of the strain rates which are also time independent (i.e. $\sigma = s(\dot{\epsilon})$). From the St. Venant hypothesis plane sections must remain plane and hence the displacement and the strain must vary linearly across the beam. Thus:-

$$\epsilon = \kappa y \quad (3.44)$$

κ is the curvature of the beam and y the distance from the neutral axis. The bending moment, M is given by:-

$$M = \int_A y s(\dot{\kappa} y) dA \quad (3.45)$$

Here A is the cross-sectional area of the beam. Once the form of the creep law and the shape of the beam cross-section have been specified this equation can be integrated. For power law creep (equation 3.34) and a rectangular beam of depth d and width b this gives:-

$$\left(\frac{M}{M_n}\right)^n = \dot{\kappa} / \dot{\kappa}_n \quad (3.46)$$

where $M_n = nbd^2\sigma_c / (4n+2)$ and $\dot{\kappa}_n = 2B/d$. B was defined in equation (3.34). Thus given the bending moment distribution $M(x)$ it is possible to determine the change in curvature and hence the deformed shape of the beam. For the cantilevered beam shown in figure 9(c):-

$$M(x) = P \cdot (\ell - x) \quad (3.47)$$

and if the deflection is not too large so that $dw/dx \ll 1$ then $\kappa = d^2w/dx^2$ and

$$\frac{\partial^3 w}{\partial x^2 \partial t} = \dot{\kappa}_n \left[\frac{P(\ell - x)}{M_n} \right]^n \quad (3.48)$$

This can be integrated using the boundary conditions $w = dw/dx = 0$ at the built-in end at $x=0$ giving

$$w = \dot{\kappa}_n \ell^{n+2} t \left(\frac{P}{M_n} \right)^n \left[\frac{(1 - (x/\ell))^{n+2}}{(n+1)(n+2)} + \frac{x}{\ell(n+1)} - \frac{1}{(n+1)(n+2)} \right] \quad (3.49)$$

The term in square brackets indicates the shape of the deformed beam which grows linearly with time. Note that this shape is in general different from the corresponding elastic case which would be given by putting $n=1$ in (3.49). This type of analysis can be readily extended to include initial elastic and plastic deformation which would simply appear as an initial deflection to be added to w from (3.49), but plastic and elastic deformations which change with time are excluded. It is possible to include variations of material properties and temperature with x and t provided the variables can still be separated and the integrals above performed analytically. Thus non-steady state solutions including ones in which the load varies with time can be generated. However the material must always be deforming in the linear region of the creep curve and the onset of ductile failure cannot be modelled with this approach. The deflections simply increase until the solution becomes invalid.

Property and temperature variations through the thickness cannot be so easily accommodated unfortunately because these would influence the position of the neutral axis and invalidate equation (3.46). If it known that brittle failure is going to dominate then this can be analysed by independently applying Kachanov's equation. From this the damage factor D can be computed over the beam and the $D=1$ surface, which will start at the outer fibres where the stress is largest, found and its progression through the beam computed. Failure will occur when there is insufficient material left to prevent plastic collapse. The failure mode appears as a crack on the tensile stress surface and propagates into the body of the beam as

shown in figure 10(a). This case was analysed analytically by Odqvist [7].

The reader should note that from this point the analytic analysis becomes much more complicated hence only the basic equations are given below. Fuller details can be obtained from the references quoted.

Statically Indeterminate Beams.

These cases are most conveniently analysed using the creep potential described in section 3.1. This can be generalised from stress/strain rate systems to moment/curvature rate systems [11]. Thus a potential ϕ per unit length of beam, can be defined such that:-

$$\dot{\kappa} = \frac{\partial \phi}{\partial M} \quad (3.50)$$

For power law creep ϕ is given by:-

$$\phi(M) = \left(\frac{M}{M_n}\right)^{n+1} \frac{\dot{\kappa}_n M_n}{n+1} \quad (3.51)$$

The potential for the whole beam Φ can be found by integrating ϕ along the beam length. To do this it will be necessary to include the redundant actions (which could be moments and/or shear forces) as unknowns. In this form the problem is identical to that of non-linear elasticity and the corresponding variational theorems can be used here. In particular it is possible to apply Castigliano's theorem [15] which relates a generalised deflection rate (or rotation rate) q , to the corresponding action Q :-

$$q = \frac{\partial \Phi}{\partial Q} \quad (3.52)$$

The redundant actions Q_1, Q_2 etc. would normally correspond to zero deflection or rotations (e.g. a beam built-in at both ends) and thus:-

$$\frac{\partial \Phi}{\partial Q_1} = \frac{\partial \Phi}{\partial Q_2} = \text{etc} = 0 \quad (3.53)$$

This will yield a set of non-linear equations from which the redundant actions can be found. The methods used in the statically determinate cases can then be applied to give the deflections throughout the beam.

Axial Force Cases.

When an axial force N , is present it is necessary to introduce the extension, ϵ_o , of the beam centerline. The St. Venant hypothesis can still be applied and thus:-

$$N = \int_A s(\dot{\epsilon}_o + \dot{\kappa}y) dA \quad M = \int_A s(\dot{\epsilon}_o + \dot{\kappa}y)y dA \quad (3.54)$$

The neutral axis is now located at the point $y=y_o$, where $\epsilon_o + \dot{\kappa}y_o = 0$. A major problem now arises in analytical analysis since these equations cannot in general be decoupled to give $\dot{\epsilon}_o$ and $\dot{\kappa}$ as functions of N and M . However two approximations are commonly used to overcome this.

In the first it is assumed that ϕ is a function of a single parameter R which has an assumed dependency on N and M . R is chosen so that when the axial force is absent $R=M$ and the pure bending case is given exactly. From equation (3.50):-

$$\dot{\kappa} = \frac{d\phi}{dR} \frac{\partial R}{\partial M} \quad (3.55)$$

Similarly

$$\dot{\epsilon}_o = \frac{d\phi}{dR} \frac{\partial R}{\partial N} \quad (3.56)$$

For power law creep $\phi(R)$ is given by:-

$$\phi(R) = \left(\frac{R}{M_n}\right)^{n+1} \dot{\kappa}_n \frac{M_n}{1+n} \quad (3.57)$$

In [11] it is shown that the best approximation is obtained when

$$R = M + \frac{k^2 N^2 d^2}{4} \quad \text{where } k = \left[\frac{n}{2n+1}\right]^{n/(n+1)} \quad (3.58)$$

This also gives exact results for the case $M=0$.

In the second approximation the decoupling of $\dot{\epsilon}_0$ and $\dot{\kappa}$ is achieved by replacing the real beam by a beam of "ideal I section" See figure 10(b). The section consists of two infinitely thin flanges separated by a web which carries the intersecting force but does not participate in the bending and axial extension. The flanges each have a finite area equal to half the real beam area and the flange separation d_I , is chosen to give the best approximation to the creep behaviour of the real beam. This idealisation means that the stresses are uniform in each flange. If these are σ_u and σ_l then:-

$$N = \frac{\sigma_u + \sigma_l}{2} A \quad M = \frac{\sigma_u - \sigma_l}{4} Ad_I \quad (3.59)$$

For a rectangular beam of depth d , and for power law creep, the power dissipations for the cases $M=0$ and $N=0$ can be made exact by choosing:-

$$d_I = d \left[\frac{n}{2n+1} \right]^{n/(n+1)} \quad (3.60)$$

For power law creep the extension and curvature rates are given by:-

$$\dot{\epsilon}_0 = \frac{B}{2} [|N' + M'|^{n-1} (N' + M') + |N' - M'|^{n-1} (N' - M')] \quad (3.61)$$

$$\dot{\kappa} = \frac{B}{2d_I} [|N' + M'|^{n-1} (N' + M') - |N' - M'|^{n-1} (N' - M')] \quad (3.62)$$

where $N' = N/(B\sigma_c)$ and $M' = 2M/(Bd_I\sigma_c)$.

An example which can be solved by these methods is illustrated in figure 11(a). Note however that the solution can only be obtained by direct integration of the equations above when the moment due to the axial force itself is small compared to the other moments. In the case shown in figure 11(a) this implies that $Nw \ll ql$. This ceases to be valid at large deflections and the problem becomes geometrically non-linear.

3.3.4. Geometrically Non-Linear Cases

Geometrical non-linearity seriously complicates the analytical treatment of creep problems because the ratio N/M changes with deformation. It is possible however to obtain solutions in some cases by making appropriate approximations. The example shown in figure 11(b) is described in detail in [11] and the main features of the method are given below. The structure shown is a beam fully built-in at both ends so that as the lateral deflection develops due to the load q , the beam must stretch axially and this produces an axial force. The solution is facilitated by using the ideal I section model, by assuming that $n=3$ (although other odd values of n can be used) in the creep power law and by assuming a particular form of the deflected shape i.e.:-

$$w = c(t) \sin (\pi x/l) \quad (3.63)$$

The extensional strain and curvature rates are:-

$$\dot{\epsilon}_0 = BN' [(N')^2 + 3(M')^2] \quad \dot{\kappa} = \frac{2BM'}{d} [3(N')^2 + (M')^2] \quad (3.64, 3.65)$$

The kinematic relations including the necessary non-linear term are:-

$$\kappa = \frac{\partial^2 w}{\partial x^2} \quad \epsilon_0 = \frac{\partial u}{\partial x} + \frac{1}{2} \left(\frac{\partial w}{\partial x} \right)^2 \quad (3.66, 3.67)$$

The bending moment M which is given by $(Nw + qlx - qx^2/2)$ is approximated by the first two terms of a Fourier series:-

$$M = Nw + \frac{16q\ell^2}{\pi^3} \sin \left(\frac{\pi x}{\ell} \right) \quad (3.68)$$

Substituting the expressions for κ , ϵ , and M into equations (3.64, 3.65) gives:-

$$\left(\frac{\pi d}{2\ell} \right)^2 \dot{c} \sin \left(\frac{\pi x}{\ell} \right) = B (1 - cN') (3(N')^2 + (1 - cN')^2 \sin^2 \left(\frac{\pi x}{\ell} \right) \sin \left(\frac{\pi x}{\ell} \right) \sin^2 \left(\frac{\pi x}{\ell} \right) \sin \left(\frac{\pi x}{\ell} \right) \quad (3.69)$$

$$\frac{\partial \dot{u}}{\partial x} + \left(\frac{\pi d}{2l}\right)^2 c \dot{c} \cos^2 \left(\frac{\pi x}{l}\right) = BN'((N')^2 + 3(1 - cN'^2 \sin^2 \left(\frac{\pi x}{l}\right))) \quad (3.70)$$

These equations can be integrated in x using the weighting function $\sin(\pi x/l)$ in the first and noting that $u = 0$ at $x = 0, l$ to give:-

$$\left(\frac{\pi d}{2l}\right)^2 \dot{c} = B (1 - cN') (3(N')^2 + \frac{3}{4} (1 - cN')^2) \quad (3.71)$$

$$\left(\frac{\pi d}{2l}\right)^2 c \dot{c} = BN' (2(N')^2 + 3(1 - cN')^2) \quad (3.72)$$

These non-linear coupled equations in c and N' can now be numerically integrated in time to give the solution which is illustrated in figure 11(c). Rabotnov in [11] was able to show that this solution converged on the separate solutions valid for either small or moderately large deflections which gave support to the approximations used. Note how the axial force, N' increases with time as the lateral deflection develops as expected but then reaches a maximum before approaching an asymptotic value. In fact the behaviour at very large deflections becomes inaccurate because of additional non-linear terms in the kinematic relations which were ignored above. This example serves to illustrate the complicated nature of analytical solutions to creep problems particularly those associated with geometrical non-linearities.

3.3.5 Axisymmetric Solids

Practical structures in this category are typified by thick-walled cylinders and solid discs under radial or tangential axisymmetric loads and their analysis is possible using analytical methods since only one space variable is involved i.e. radius. The general methods will not be described here but one of the examples analysed by Rabotnov [11] may be of use in evaluating approximate methods. In this he considers the failure by creep of a rotating solid disc using three methods to evaluate the expected failure life. The results are compared with a series of test measurements.

The stress distribution in the disc is statically indeterminate and changes with time making life prediction difficult. However because the problem has only one space dimension an "exact" solution is possible within the limitation of small deflections (in this case this means that the

deflections must be small compared to the radius and that the transverse strains should be small so that significant thinning does not occur). In the approximate methods the stress distribution is assumed constant with time and corresponds to either (a) elastic behaviour or (b) ideal plastic behaviour. In case (b) this corresponds to a limiting case of power law creep where $n \rightarrow \infty$, and the stress distribution is simply $\sigma_\theta = \text{constant}$.

The results of all three methods were compared with the experiments by using the maximum stress predicted together with a cumulative damage law to predict creep failure from standard uniaxial test results on bars. The "exact" method gave good results, typically within 5% of the experimental results. The plastic approximation gave reasonable results (within 30% in general), and for very ductile creep failures where the limitation of small deflection was violated, was comparable with the "exact" method. The elastic method gave the largest errors in general (predicted stress up to 1.9 times too high) but, as expected, gave reasonable results (within 30%) when the failure mode was brittle creep.

3.3.6 Plates and Shells

Only a very limited number of analytical solutions exist for creep of plate and shell structures. The basic problem arises from the nature of the creep potential function ϕ described in stress and strain rate terms in section 3.1. To have any chance of analysing plates and shells it is necessary to formulate the function ϕ in terms of the plate or shell stress resultants i.e. the moments M_{ij} and the membrane forces T_{ij} , where $i=1,2$ and $j=1,2$ correspond to orthogonal directions in the plane of the shell or plate. The alternative would be to consider the problem as a general solid and deal in terms of individual stresses throughout the thickness of the plate or shell which would result in impractical spatial variations. However the resulting function $\phi(M_{ij}, T_{ij})$ exists in six dimensional space for which only certain regions have known solutions.

It is instructive to note here that a similar problem arises in pure plastic analysis of plates and shells but there it is usually only required to find the collapse load i.e. the combinations of M_{ij} and T_{ij} which lie on the $\phi = \text{constant}$ surfaces, the exact form of the deformation i.e. the direction of the normal to the $\phi = \text{constant}$ surfaces, is of secondary

importance. Limits on this collapse load can be readily found by bounding $\phi(M_{ij}, T_{ij})$ with simple surfaces from within or without to give lower and upper bounds respectively. By contrast in the creep problem the initial target is normally to predict the deformation rates which requires knowledge of the true ϕ surfaces. Thus analytical solutions are only possible for specific combinations of M_{ij} and T_{ij} and even these usually involve some numerical integration of the resulting equations. To illustrate this two important cases taken from [11] are described below.

Creep of a circular plate in bending

In this case a plate loaded normally and axisymmetrically is considered in which the creep deformation is steady state and the deflections are small (in this case less than the plate thickness) so that the in-plane membrane forces, T_{ij} , can be ignored. Thus M_{ij} and T_{ij} reduce to a radial moment M_r , and a circumferential moment M_θ ($M_{r\theta} = 0$ by symmetry), which for a Von Mises multi-axial creep theory must obey:-

$$M_r = (4/3) (M_o / \dot{\kappa}_o) [\dot{\kappa}_r + \frac{1}{2} \dot{\kappa}_\theta] \quad (3.73)$$

$$M_\theta = (4/3) (M_o / \dot{\kappa}_o) [\dot{\kappa}_\theta + \frac{1}{2} \dot{\kappa}_r] \quad (3.74)$$

$$M_o^2 = M_r^2 + M_\theta^2 - M_r M_\theta \quad (3.75)$$

$$\dot{\kappa}_o^2 = (4/3) [\dot{\kappa}_r^2 + \dot{\kappa}_\theta^2 + \dot{\kappa}_r \dot{\kappa}_\theta] \quad (3.76)$$

κ_r and κ_θ are the radial and circumferential curvatures respectively and the kinematic relations are:-

$$\dot{\kappa}_r = \frac{d^2 \dot{w}}{dr^2} \quad \dot{\kappa}_\theta = \frac{1}{r} \frac{d \dot{w}}{dr} \quad (3.77, 3.78)$$

w is the normal deflection and can be eliminated to yield the compatibility condition

$$\frac{d}{dr} (r \dot{\kappa}_\theta) - \dot{\kappa}_r = 0 \quad (3.79)$$

The equations of equilibrium are:-

$$\frac{d}{dr} (rM_r) - M_\theta + rN_r = 0 \quad (3.80)$$

$$\frac{d}{dr} (rN_r) + qr = 0 \quad (3.81)$$

N_r is the shear force in the plate and q the distributed normal load. Thus the seven unknowns M_r , M_θ , M_o , k_r , k_o , k_θ , N_r can be found by integrating with radius, r , the seven equations above and applying the appropriate boundary conditions. Note that this gives a universal solution, i.e. independent of material creep law. This is a common feature of steady state creep problems [11]. However the interpretation of the solution in terms of deflection etc. requires the creep law and its parameters to be inserted a-posteriori. For example the central deflection rate \dot{w} for a freely supported plate of radius b and thickness d under a uniform load q and made from a material obeying power law creep with $n=3$ is given by:-

$$\dot{w} = 0.87 \times 10^{-3} (Bd^2/32b)(qb^2/M_n)^3 \quad (3.82)$$

Creep of Moment-free Axisymmetric Shells

This example represents an important class of structures in which solutions to the creep problem are practical since the resultants M_{ij} , T_{ij} reduce to a meridional force N_1 , and a circumferential force N_2 . See figure 12. The equations of equilibrium are [11]:-

$$\frac{dN_1}{ds} + \frac{N_1 - N_2}{r} \sin(\theta) + q_1 = 0 \quad (3.83)$$

$$\frac{N_1}{R_1} + \frac{N_2}{R_2} + q_n = 0 \quad (3.84)$$

$R_1 = -ds/d\theta$ is the radius of curvature in the meridional direction and $R_2 = r/\cos(\theta)$ the one in the circumferential direction. q_n is the pressure normal to the shell surface and q the traction along the meridian. If the deflections are small the equations above are linear in N_1 and N_2 and can be solved to give:-

$$N_1 = - \frac{1}{r \cos \theta} \int r (q_n \sin \theta + q_1 \cos \theta) ds$$

$$N_2 = - (R_2/R_1)N_1 - R_2 q_n \quad (3.86)$$

This direct solution for N_1 and N_2 reflects the fact that axisymmetric moment-free shells are statically determinate. The kinematic relations are:-

$$\epsilon_1 = \frac{du}{ds} - \frac{w}{R_1} ; \epsilon_2 = \frac{1}{r} (u \sin \theta - w \cos \theta) \quad (3.87, 3.88)$$

ϵ_1 and ϵ_2 are the meridional and circumferential extension strains respectively and u and w are the corresponding deflections. Using the creep law in the form $\dot{\epsilon} = \dot{\epsilon}_n v(\sigma/\sigma_c)$ and applying the Von Mises theory for a shell of thickness d , gives:-

$$\dot{\epsilon}_1 = \dot{\epsilon}_n v(N_0/(d\sigma_c)) [N_1^{-1/2} N_2] / N_0 \quad \dot{\epsilon}_2 = \dot{\epsilon}_n v(N_0/(d\sigma_c)) [N_2^{-1/2} N_1] / N_0 \quad (3.89, 3.90)$$

where
$$N_0^2 = N_1^2 + N_2^2 - N_1 N_2 \quad (3.91)$$

Thus the strain rates can be found and the corresponding displacements computed from:-

$$u = \cos \theta \int (\epsilon_1 - \frac{R_2}{R_1} \epsilon_2) ds / \cos \theta \quad (3.92)$$

$$w = u \tan \theta - R_2 \epsilon_2 \quad (3.93)$$

It should be emphasised that the solutions obtained in this way are only valid while the deflections are small compared to the radii of curvature and while the shell thickness remains sensibly constant. Thus the full analysis of a large deformation ductile creep failure would be impossible with this method.

3.4 Numerical Methods

3.4.1 Introduction

It is evident from the previous section that structural problems involving creep are very difficult to solve analytically. This, together with the advances in recent years of computer hardware has prompted the development of many numerical methods which are capable of handling such problems. The methods fall into three categories viz. finite difference, finite element and boundary element methods. In the finite difference method the basic equations describing the deformation of the structure are expressed in equations which are solved by discretisation in terms of the co-ordinates of the mesh nodes. In the finite element method the structure is divided into a set of elements interconnected at a FINITE number of nodes. The displacement is approximated by analytic functions within each element and the problem is expressed in terms of the nodal displacements. In the boundary element method a similar set of elements is produced but the structural equations are expressed in terms of functions on the surface of each element.

The methods were all originally developed for linear structural problems but many versions are now available which support non-linear features in particular the effects of large deflections and material non-linearities of plasticity and creep.

It should be noted that all the methods require large computer codes which may be difficult, or even impossible, to interface with other codes which may be used to model the non-structural parts of severe accidents.

Although increasing in popularity the boundary element method is still very little used at present and has not been considered further in this study. The finite element method is by far the most popular at present, mainly because it permits a much wider choice of structure shape and topology to be modelled compared with the finite difference method. However this generality comes at the expense of certain limitations in the behaviour of some elements which can lead to errors if incorrectly used. Thus finite difference codes still have a role to play and one major code (BOSOR) is described below.

All the methods use the basic principles described for the analytical methods in section 3.1 i.e equilibrium, compatibility and a constitutive law, although the equilibrium condition is commonly expressed in an equivalent variational form. Generally the methods involve large computer codes which in most cases have been developed by specialist organisations on a commercial basis. Thus the user would not normally have access to, or detailed knowledge of all aspects of the method, but he must be wary of any limitations which may not always be advertised by the code developers. In particular for severe accident studies the potential user of any particular code must bear in mind the following points before undertaking an analysis:-

- (1) The types of structure that can be analysed.
- (2) The form of the creep or constitutive law used and what temperature variations are permitted.
- (3) The form of the strain/displacement relations used and whether these include the appropriate non-linear terms to account for effects such as out-of-plane stretching and transverse thinning of plates and shells.
- (4) The compatibility of the results presented with the appropriate failure criteria so that a failure as well as a creep analysis can be performed if desired.

3.4.2 Finite Difference Code BOSOR

BOSOR (Buckling Of Shells Of Revolution) is a series of codes that have been developed by Bushnell [16] initially for buckling analysis of thin shells used in the aerospace industry, but for more general applications in later versions. The code represents the displacement of shell structures using a finite difference mesh in the meridional direction together with a Fourier series in the circumferential direction. This semi-analytic approach restricts the analysis to axisymmetric shells (non-axisymmetric loads are permitted but only for linear analyses) but is otherwise very general and has been widely used and verified against experimental results. Of particular interest here is the version BOSOR5 which includes the effects of large deflections, plasticity and creep.

The creep law used in BOSOR5 is of the form:-

$$\dot{\epsilon}_c = B\sigma^m t_e^n \quad (3.94)$$

Here B, m and n are material constants and t_e is an effective time which can be used to allow the strain rate to exhibit time hardening or strain hardening behaviour. Putting $n=0$ gives the simple power law creep used in the analytical analyses above. To allow for temperature variations in time and space it would be necessary to vary the parameter B accordingly. This does not appear to be a feature of the version described in [15] but could, in principle, be easily coded.

Equilibrium is expressed by the equivalent Principal of Virtual Work [15]:-

$$\delta U = \int_{vol} \{\epsilon - \epsilon_p - \epsilon_c - \epsilon_T\} [D] \{\delta\epsilon\} dV = \delta W \quad (3.95)$$

U is the shell strain energy over its whole volume V and W is the work done by the external forces. ϵ , ϵ_p , ϵ_c and ϵ_T are the total, plastic, creep and thermal strains respectively and D is the elastic stiffness matrix. If the N degrees of freedom of the finite difference mesh are q_i , then for equilibrium:-

$$\int \{\epsilon - \epsilon_p - \epsilon_c - \epsilon_T\} [D] \left\{ \frac{\partial \epsilon}{\partial q_i} \right\} dV - \frac{\partial W}{\partial q_i} = 0 \quad (i = 1, 2, 3 \dots N) \quad (3.96)$$

This gives a set of non-linear equations in q_i which are solved iteratively in BOSOR5 using the Newton-Raphson method. The mesh can have nodes both along the meridian and through the thickness of the shell so that the progress of any plasticity through the structure can be fully modelled. The St. Venant hypothesis is used to reduce the total strain variation through the thickness to four components viz. membrane extensions and curvatures in both directions. The strain components in equation (3.96) are expressed in terms of the displacements by assuming that (1) the creep and thermal strains are independent of q_i and can thus be treated as initial strains and (2) the plastic strains are determined by the "tangent stiffness" method which allows the plastic strain to be determined from the slope of the plastic stress strain curve (assumed to be in the form of a

set of experimental points ϵ_p, σ). The total strain includes non-linear terms which allow for out-of-plane stretching and should allow for transverse thinning although the latter was not represented in the examples given in [16].

To obtain the solution the loads or time steps are applied in increments and a "subincremental" method is used. Thus each load or time increment is divided into a set of subincrements in which the plastic and creep strains can vary while the load is held constant. This increases the reliability with which problems involving non-linear plastic and time dependent material behaviour can be solved and greatly reduces the number of load increments and the computer time needed for satisfactory results. Compared to the finite element codes described below BOSOR5 is a relatively small code (~ 10000 program lines) which could be adapted to interface with other programs.

3.4.3 Finite Element Methods

It is not possible here to describe the finite element method or the codes (of which some 500 now exist) based on it in any great detail. Attention will be restricted to a brief outline of the method and the codes and any aspects of particular relevance to severe accident studies. Further details can be obtained from the theoretical text by Zienkiewicz [17], the relevant user and theory manuals, and the review of general purpose finite element codes by Fong [18].

The equilibrium of a structure can be formulated by considering its potential energy Φ which is given by:-

$$\Phi = U - W \quad (3.97)$$

U is the strain energy and W the work done by the external forces. Equilibrium occurs when Φ has its minimum value which becomes a variational problem when, as in the finite element method, U is an integral of unknown functions. U is expressed in terms of nodal displacements, q_i , and the displacement field within each element.

Each element displacement field is described by functions (known as shape functions) and the values of q_i at the nodes attached to that element.

These shape functions are simple analytic functions, commonly polynomials, which can be integrated using Gaussian quadrature to give U in the form:-

$$U = \frac{1}{2} \{q_i\}^T [K] \{q_i\} \quad (3.98)$$

[K] is the stiffness matrix and in the simple linear elastic case the solution is given by:-

$$\{q_i\}^T = [K]^{-1} \{Q_i\} \quad (3.99)$$

Here Q_i are the forces applied at the nodes.

The method is very versatile and can, in principle, be used to model any structural problem. However limitations do exist, and the user should be particularly aware of:-

- (1) The choice of shape function can affect the solution and some elements, notably plate and shell elements, can give spurious results in certain cases. If in doubt, it is necessary to perform element tests to check for convergence, compatibility and stability.
- (2) It is easy, particularly with the automatic mesh generators now normally used, to generate a well defined problem which cannot be solved because it would be impractical due to excessive requirements of either computer core storage, disc storage or processor time. This is particularly true for non-linear problems and a rough check (based on the anticipated band-width and number of load increments etc.) should be made of the likely computational resources needed before proceeding.

It is clear that quality assurance is important in connection with these analyses and an organisation NAFEMS (National Agency For Finite Element Methods and Standards) has been set up to assist in this [19]. In particular NAFEMS have produced a set of bench-marks for testing the methods although at present these are limited to linear cases. Culham is a member of NAFEMS. Also in connection with this problem research into a-posteriori error analysis is underway, which if successful should provide

a systematic way of checking whether the solution obtained from a finite element analysis is correct.

Some aspects of the codes which are likely to be of interest here are described below.

PAFEC (PAFEC Ltd., Strelley Hall, Strelley, Nottingham NG8 6PE)

The development of this code started at the University of Nottingham in 1965 and since 1976 has been continued by PAFEC Ltd. The code is widely used in the U.K. and is the only finite element code currently available on Culham computers. The code includes a creep law which can be expressed as a general function of the form $\dot{\epsilon}_c = f(\sigma, t, \epsilon)$ using a user supplied subroutine, but general temperature variations cannot be easily accommodated - only element to element variations in the creep constant are allowed. It has a comprehensive range of elements and geometrically non-linear and plasticity as well as creep problems can be solved. Unfortunately no two of these can be combined within a single analysis and thus the code is of limited use for the present study.

The following codes have all been developed in the USA, are used worldwide and include general purpose facilities notably large deformation, plasticity and creep.

ANSYS (SASI, Johnson Road, P.O. Box 65, Houston Pa 15342)

This code has been developed since 1972 by Swanson Analysis Systems Inc. It is aimed mainly at the nuclear industry and is very popular because of its user-friendliness although some limitations have been found in certain elements. One general relevant limitation here is that it cannot be used for large strain analysis. This means that whilst large deformation can be modelled, such as out-of-plane stretching of plates and shells, if these result in large strains the method is invalid and cannot be used for example to model the effects of cross-sectional thinning or necking.

ABAQUS (Hibbitt, Karlson and Sorensen Inc., 35 South Angell Street,
Providence, Rhode Island 02906)

This is a relatively new code developed since 1979 mainly for the oil and nuclear industries. It is a powerful code, rapidly becoming popular, and is currently available on the CRAY2 at Harwell. It includes fluid/structure interaction which may be of use in severe accident studies. It does not appear to have any limitations which would restrict its use here although examination of the user manual indicates that the general non-linear material facilities cannot be used with general shell elements - only axi-symmetric shell elements. It has automatic load incrementing facilities and user defined subroutines for non-linear material properties.

ADINA (ADINA Engineering Inc., 71 Eiton Avenue, Watertown, Massachusetts 02172)

This was developed by Professor Bathe of M.I.T. in 1976 for general applications and is now marketed by ADINA Engineering Inc. It has only a small element library, although this should not be a limitation here, and includes fluid/structure interaction. It is aimed at the more academically orientated users who in the past have obtained the source code and adapted it to suit in-house facilities.

MARC (MARC, 260 Sheridan Avenue, Suite 314, Palo Alto, California 94306)

MARC has been developed since 1971 and is aimed at the nuclear industry. It appears to have no limitations of particular relevance here although it is not as widely used as the other codes. It does have user defined subroutine facilities for non-linear material properties.

Before using any of the codes in a severe accident study it would be necessary to compare facilities offered at the time (since the codes are continually developing) with the requirements of the study, in great detail. In particular the limitation found with PAFEC, with which the author is familiar, concerning permitted temperature variations may also exist in other codes.

4. MATERIALS DATA

It is not possible here to provide comprehensive data for all the materials under all appropriate conditions. Firstly there would be logistical problems, secondly not all the existing data is available in the open literature and finally some regions of interest here are of no concern in the design basis conditions which largely dictate what material tests are done. Thus the intention here has been to present "generic" data which can be used in a wide range of severe accident studies. Then if necessary individual studies could be refined by using data more closely matched to specific examples or from data generated especially for this work.

In particular all the data given below are for unirradiated materials. It is known that neutron irradiation influences the mechanical properties of all materials in ways that depend on the neutron dose and on the irradiation temperature - in some cases the behaviour is complicated and difficult to quantify. Notably the creep ductility of structural materials is reduced by prolonged exposure to neutron irradiation and this may influence their high temperature failure mode in a severe accident [20]. Thus the material properties needed to analyse a severe accident which occurred towards the end of a reactor's design life may be different from the non-irradiated properties below which would correspond to a severe accident early on in a reactor's design life.

The reactor components of interest here are the reactor vessel and the internal core supports. In an LMFBR the operating temperature is high (up to 650°C) but stresses can be kept relatively low since the internal pressure is small (<1 MPa). For these reasons, and because of their corrosion resistance, austenitic stainless steels are used for both vessel and internal structures. The types used are AISI 304 or 316. The internal structures of a PWR are also made from these materials (304 in the case of Sizewell B) primarily because of corrosion resistance. The high internal pressure (15 MPa) in a PWR however demands a stronger material for the pressure vessel but one which only needs to operate at a relatively low temperature (<320°C). For these reasons ferritic steels are used here (AISI 508 series) which derive their high strength at moderate temperatures from a precipitation of carbides of the minor alloying constituents (e.g. Cr, Ni, Mn or Mo). Water-side corrosion resistance is achieved by cladding the inside of the vessel with a thin layer of stainless steel. The bottom

head of a PWR is penetrated by instrument tubes which may play a part in the course of a severe accident. These are manufactured from Inconel (type ASME SB166 or 167 (also known as Inconel 600) in the case of Sizewell B) containing 15% Cr 8% Fe and 75% Ni.

From section 3.3 it was noted that a reasonable model of material behaviour at high temperature can be obtained from simple constitutive and damage laws :-

$$\epsilon = (\sigma/\sigma_p)^m + \int B(\sigma/\sigma_c)^n dt \quad (4.1)$$

$$dD/dt = [\sigma/(1-D)]^v \sigma_k^{-v} t_k^{-1} (1+v)^{-1} \quad (4.2)$$

Here σ_p , B and σ_k are temperature dependent, and σ_c and v are temperature independent, material properties (t_k is introduced to simplify the units in the damage equation and here $t_k = 3.6 \times 10^8$ seconds). The temperature variation of B can be fitted to the Dorn equation described in section 3.2 i.e.:-

$$B = \exp(-Q/RT) \quad (4.3)$$

T is the absolute temperature in Kelvins, R is the universal gas constant (8.314×10^{-3} kJ/mole.K) and Q the activation energy which characterises the creep process. In table 1 a tentative list of these parameters is given for 304 and 316 stainless steels, a generic low alloy ferritic steel and Inconel, based on data obtained from the references cited in the table. When applying these parameters the following points should be noted:-

- (1) The choice of parameters for the stainless steels and Inconel is made relatively simple since these materials exist as single phases over all temperatures up to melting. This partly accounts for their suitability for design basis use at moderately high temperature (<1000°C) and hence the abundance of creep data on them.
- (2) By contrast the ferritic steels used in PWR pressure vessels undergo a phase change at 700-800°C ($\alpha \rightarrow \gamma$) and are not designed for use above 600°C. This is below the creep range and thus very little creep data exists on these steels. The parameters quoted in the table have

therefore been based on the ferritic steels 1%Cr-Mo-V and 2¼%Cr-1%Mo which are well described in [2]. This approach seems justified since for temperatures above the phase transition, which is the region of primary interest here, all low alloy ferritic steels loose their intrinsic "low temperature" strength. Their properties then become similar to pure iron in its γ phase and it is from this material which the data in [2] has been derived for low alloy steels at high temperatures.

- (3) The variation with temperature of the 0.2% proof stresses (P.S.) has been based on an assumed constant scaling factor between it and the dynamic fracture stress, σ_{DF} , which is given for all temperatures in [4] or [5]. The value of σ_p is given by inserting $\epsilon_p = 2 \times 10^{-3}$ (i.e. 0.2%) and $\sigma = \text{P.S.}$ in the plastic power law i.e.:-

$$(\sigma_p)^m = (\text{P.S.})^m \times 2 \times 10^{-3} \quad (4.4)$$

- (4) The brittle creep properties are based on the measurements of σ_k at the temperatures indicated. For 304 stainless steel the property of the similar grade 321 has been taken and the low alloy ferritic steel in the α phase is based on the 1%Cr, 0.75%Mn, 0.35%Mo, 0.25%Si, 0.15%C alloy in [6]. The variation of σ_k with temperature has been modelled by comparing the brittle creep failure time, t_B , based on the assumption $t_B \dot{\epsilon}_c \approx \epsilon^*$, a constant (see section 3.2) with the failure time given by the Kachanov model (see section 3.3) i.e.:-

$$t_B \approx \epsilon^* (\dot{\epsilon}_c)^{-1} \approx (1+\nu)^{-1} C^{-1} \sigma_o^{-\nu} = t_k (\sigma_k / \sigma_o)^\nu \quad (4.5)$$

It is further assumed that $\dot{\epsilon}_c$ follows an exponential variation with temperature i.e. $\dot{\epsilon}_c = A \sigma_o \exp(-Q_B/RT)$ where A is a constant and Q_B is the activation energy for brittle creep taken from [2]. Hence

$$\sigma_k = \sigma_{ko} \exp(+Q_B/\nu RT) \quad (4.6)$$

where σ_{ko} is a constant.

- (5) The values for σ_c have been obtained by fitting equations (4.1) and

(4.3) to data given in [2] or [6].

- (6) The values for m and v are based on the approximation given in [6], i.e. for many materials $m \approx 0.9 n$ and $v \approx 0.7 n$.
- (7) In the absence of complete data on Inconel 600 the activation energies Q and Q_B are based on pure nickel, and n is based on Nimonic 75 which has similar properties to Inconel 600;
- (8) All data are based on materials in their annealed condition with the exception of the low alloy steel which in the α phase is heat treated to give it characteristic strength at moderate temperatures.

5. RECOMMENDATIONS

Four approaches are summarised below which can be used to estimate the response of a structure in a severe accident.

Empirical Approach

This is the simplest possible method and can be used at an early stage in a severe accident study to estimate the response. Its accuracy may be in doubt and would normally be checked by a more lengthy analysis undertaken later. The inputs to an empirical approach are:-

- (1) An estimate of the temperature and loads on the structure and their time/space variations.
- (2) The relevant material data.
- (3) An estimate of the stresses in the structure.

The stress estimate should be made and processed in two ways. Firstly fully elastic behaviour can be assumed. The stresses can then be calculated using standard techniques. The creep life of the structure can then be estimated from stress/temperature/life correlations and a cumulative damage law as described in section 2.4. This is essentially the classical design basis approach, recommended in the design codes, and is usually associated with creep correlations based on the Larson-Miller parameter. Here however it would be more appropriate to consider using the Manson-Succop or the Dorn parameters. The possibility of the structure surviving the accident (i.e. creep life longer than accident duration) and the possibility of failure by melting should be included.

The consistency of this approach should then be checked by estimating the strain at failure from either the constitutive law or a deformation mechanism map for the material. The map should also be used to check that the analysis has not been invalidated by crossing of mechanisms boundaries during the accident. If the failure strain is small then the stresses will indeed have been elastic and the method consistent. The definition of "small" will depend on the nature of the structure, and for example would correspond to deflections out-of-plane being less than the thickness for a

laterally loaded plate or built-in beam. Small strain creep failures correspond to low stresses and long exposure times to high temperatures where brittle failure is to be expected. In a severe accident however it is more likely that the strain at failure would be large and this would in general negate the elastic approach. The elastic approach would still give valid results however if at large strains the stresses remained unchanged e.g. for a bar in tension at moderate deflection.

If invalidated the elastic approach should be supplemented by an estimate of the stresses based on fully plastic behaviour. This corresponds to a large ductility approximation and the resulting stress estimates can then be processed as for the elastic case. Consistency in this case will now correspond to strains at failure being large. The practicality of a fully plastic analysis will depend on the details of the structure but many solutions exist (e.g. [21]).

The empirical approach has the advantage of decoupling the structural and creep effects and allows rapid estimates of the creep life to be made. The refinements described above should add little to the complexity when compared with the classical design basis approach, and give further information about the mode and deformation at failure.

Analytical Approximations

In effect the empirical method above estimates the response of a structure by using the response of uniaxial creep tests under similar conditions of local stress and temperature. It would be expected to give good results when the failure mode is by brittle creep or by ductile creep in which the stresses are uniform across the structure thickness. The analytical methods described in section 3.3 provide a more fundamental approach which combines material and structural behaviour. For homogeneously stressed structures a comprehensive analytical treatment is possible and the results are given in appendix 1.

For other structures, notably plates and shells and all geometrically non-linear structures, the analytical approach is very complex and rather severe restrictions have to be applied to facilitate solutions. It would be necessary to judge the usefulness of these against specific examples of severe accident studies.

Numerical Methods

The general purpose Finite Element codes (notably ANSYS, ABAQUS, ADINA and MARC) and the axisymmetric Finite Difference code, BOSOR, offer facilities which cover the regions of interest here. It is questionable however whether their potential modelling accuracy would be justified here in view of (1) the difficulties of interfacing such large codes (particularly the Finite Element ones) with the rest of the severe accident analysis, which in itself would require large computer codes and (2) the limited material data available. They may however be of use in stand-alone calculations if the accuracy of other methods available is in doubt. It is noted that ABAQUS is available on the Harwell Cray 2 computer.

Physical Models

Very little attention is paid now to estimating structural responses using physical models.. This is mainly due to the recent improvements to the numerical methods described above which have largely displaced other approaches. However physical models can still be of use and, as in this case where the structural behaviour can be very complex, may offer advantages over the numerical methods in terms of speed, accuracy and cost. Physical models can also give insights into structural and material behaviour which may be overlooked in other methods. In the severe accident applications here, a physical model would have to be scaled down to a manageable size and it may also be desirable to change the material to one with a low melting point (e.g. lead). This would permit creep behaviour to occur at modest temperatures. It would be necessary to check that the change in scale and material does not change the failure mode. This problem is often encountered in physical modelling and is discussed by Baker [22] and Booth et al [23].

In conclusion it is recommended that the empirical approach should be used as a first stage in estimating the response of a structure in a severe accident. The self-consistency of this approach should then be checked and the failure mode and deformation at failure estimated.

It is also recommended that a further method should be used to verify the results of this by using either analytical methods, numerical methods or physical models. These additional methods are considerably more complex

than the empirical one and the choice will depend on factors beyond the scope of this study, in particular the details of the severe accident and the desired accuracy of the results.

Future Work

Following this review the next stage should be to verify whether the methods recommended are practical and verifiable. Although this could be done against artificial bench-marks it would be better to consider specific examples of severe accidents provided these were not too complicated.

Acknowledgements

The author gratefully acknowledges the helpful support from Dr K A Moore and C J Upson, and the supervision from Dr B D Turland in this work.

REFERENCES

- [1] Roberts, J.T.A. Structural materials in nuclear power systems. Plenum press. New York 1981.
- [2] Frost, H.J. and Ashby, M.F. Deformation mechanism maps for pure iron, two austenitic stainless steels, and a low alloy ferritic steel. "Fundamental aspects of structural alloy design" R.J. Jaffe and B.A. Wilcox (e.d.) Plenum press New York (1977) pp27-65.
- [3] The Fulmer optimiser. Fulmer Research Institute 1979.
- [4] Ashby, M.F., Gandhi, C. and Taplin, D.M.R. Fracture mechanism maps and their construction for f.c.c. metals and alloys. Acta Metallurgica vol 27 pp699-729. 1979.
- [5] Fields, R.J., Weerasooriya, T. and Ashby, M.F. Fracture mechanisms in pure iron, two austenitic stainless steels and one ferritic steel. Met. trans. ASME vol 11A 1980 p333-342.
- [6] Odqvist, F.K.G. Mathematical theory of creep and creep rupture. Oxford Clarendon press 1974.
- [7] Odqvist, F.K.G. and Hult, J. Ark. Fys. 19, 379,1961.
- [8] Robinson, E.L. Trans. Am. Soc. Mech. Engrs. Vol.74, pp.777-81 1982.
- [9] Orr, R.L., Sherby, O.D. and Dorn, J.E. Trans. A.S.M. 46(1954) 113
- [10] Love, A.E.H. A treatise on the mathematical theory of elasticity. New York, Dover Publication, 1944.
- [11] Rabotnov, Yu N. Creep problems in structural members. North Holland 1969.
- [12] Gittus, J. Creep, viscoelasticity and creep fracture in solids. Applied Science Publishers Ltd. 1975.

- [13] Oding, J.A. (ed) Creep and stress relaxation in metals. Oliver & Boyd 1965.
- [14] Clauss, F.L. An examination of high temperature failure stress rupture correlating parameters. Proc. ASTM 60 (1960).
- [15] Timoshenko, S and Goodier, J.N., Theory of elasticity. McGraw-Hill 1951.
- [16] Bushnell, D. A strategy for the solution of problems involving, large deflections, plasticity and creep. Int. J. Num. Meth. Eng. Vol.II 683-708 (1977).
- [17] Zienkiewicz, O.C. The finite element method in engineering science. McGraw-Hill (1971).
- [18] Fong, H.H., A Comparison of eight general purpose finite element computer programs. Chapter in structural mechanics software series - V (ed W D Pilkey) University Press of Virginia, Charlottesville 1983
- [19] Mair, W.M. The objectives of the national agency for finite element methods and standards. National Engineering Laboratory report WM6C, February 1984.
- [20] Bloom, F.E. and Weir, J.R. Effect of neutron irradiation on the ductility of austenitic stainless steel. Nuc. Tech. Vol.16 pp.45-54 October 1972.
- [21] Bickell, M.B. and Ruiz, C. Pressure vessel design and analysis. McMillan, St. Martin's Press, New York 1967.
- [22] Baker, W.E. Modelling the blast response of structures using dissimilar materials. AIAA J. Vol.7, No.5, May 1969.
- [23] Booth, E, Collier, D and Miles, J. Impact scalability of plated steel structures, Structural Crashworthiness, ed. Jones N and Wierzbicki T, Butterworths 1983.

- [24] Metals Handbook Ninth Edition Vol. 3. Properties and Selection of Stainless Steels, Tools Materials and Special Purpose Metals. ASM (1980).
- [25] Inconel Alloy 600 data sheet. Wiggins alloys Ltd. Publications 3269 November 1981.
- [26] Brandes E A. Smithells Metals Reference Book, 6th edition, Butterworths 1983.

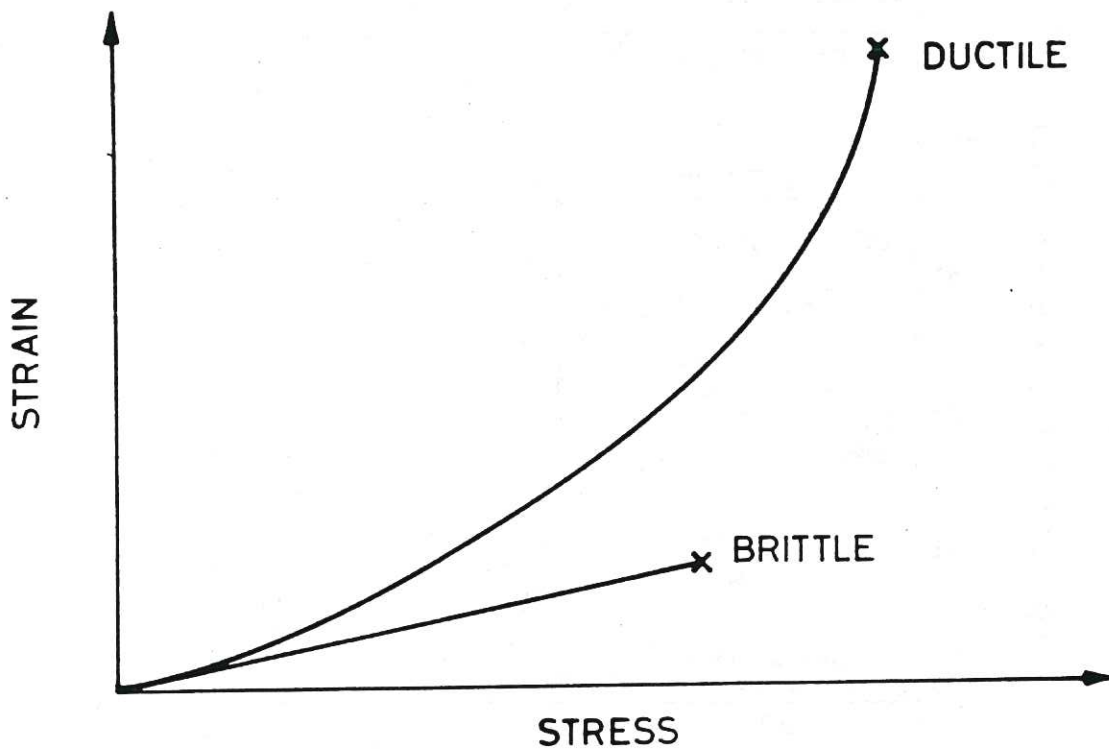
Table 1

MATERIAL PROPERTIES

	Units	304 Stainless Steel	316 Stainless Steel	Low Alloy Ferritic Steel α phase γ phase		Inconel 600	
Temperature Range Reference	K	300/1680 [2]	300/1680 [2]	300/1033 [2]	1033/1753 [2]	300/1666 [4]	Room temp./ phase change/ melting point
σ DF Reference	MN/ m ²	1194/127 [5]	1061/100 [5]	1194/587 [5]	587/89 [5]	1000/152 [4]	Note 3
0.2% P.S. Reference	"	235/25 [24]	275/26 [24]	600/295 [3]	295/45 [3]	276/42 [25]	Note 3
σ P	"	590/63	659/62	1897/932	932/142	3452/525	Note 3
σ (t = k k 3.6x10 ⁸) Reference Temperature	"	14.7 [6] 800°C	10.8 [6] 815°C	11.8 [6] 600°C	2.71 [5] 1000°C	1.17 [25] 980°C	Note 4
Q B Reference	kJ/ mole	167.4 [2]	167.4 [2]	173.7 [2]	159.0 [2]	133.9 [2]	Note 7
σ ko	MN/ m ²	0.41	0.38	0.04	0.076	0.00140	
Q Reference	kJ/ mole	279.6 [2]	279.6 [2]	251.1 [2]	269.9 [2]	282.0 [26]	Note 5, 7
σ c Reference	MN/ m ²	7.25 [2]	10.3 [2]	6.7 [2]	11.2 [2]	0.724 [6]	
n Reference		7.5 [2]	7.9 [2]	6.0 [2]		2.73 [2]	Note 6, 7
m		6.75	7.11	5.4		2.46	
v		5.25	5.53	4.2		1.91	

NB Notes 3-7 appear on page 46 of the main text

(a) TIME INDEPENDENT FAILURE



(b) TIME DEPENDENT (CREEP) FAILURE

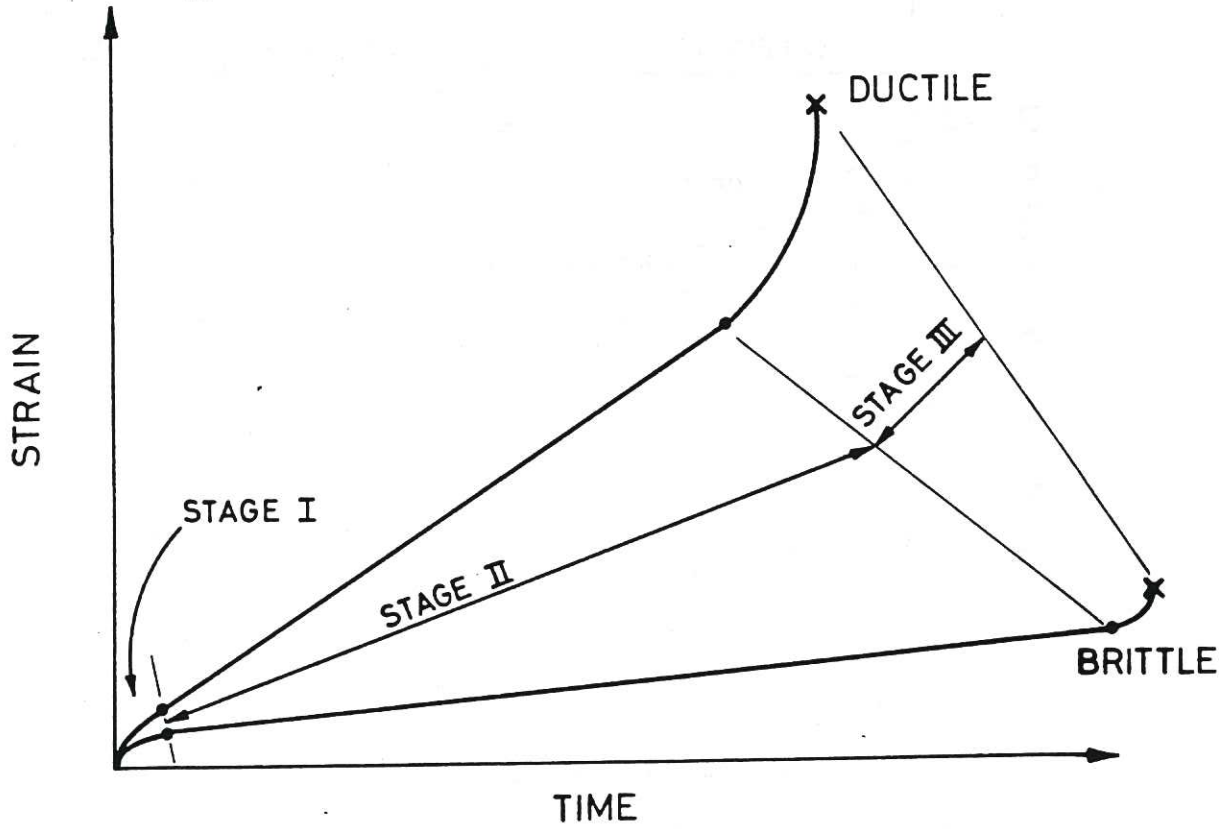
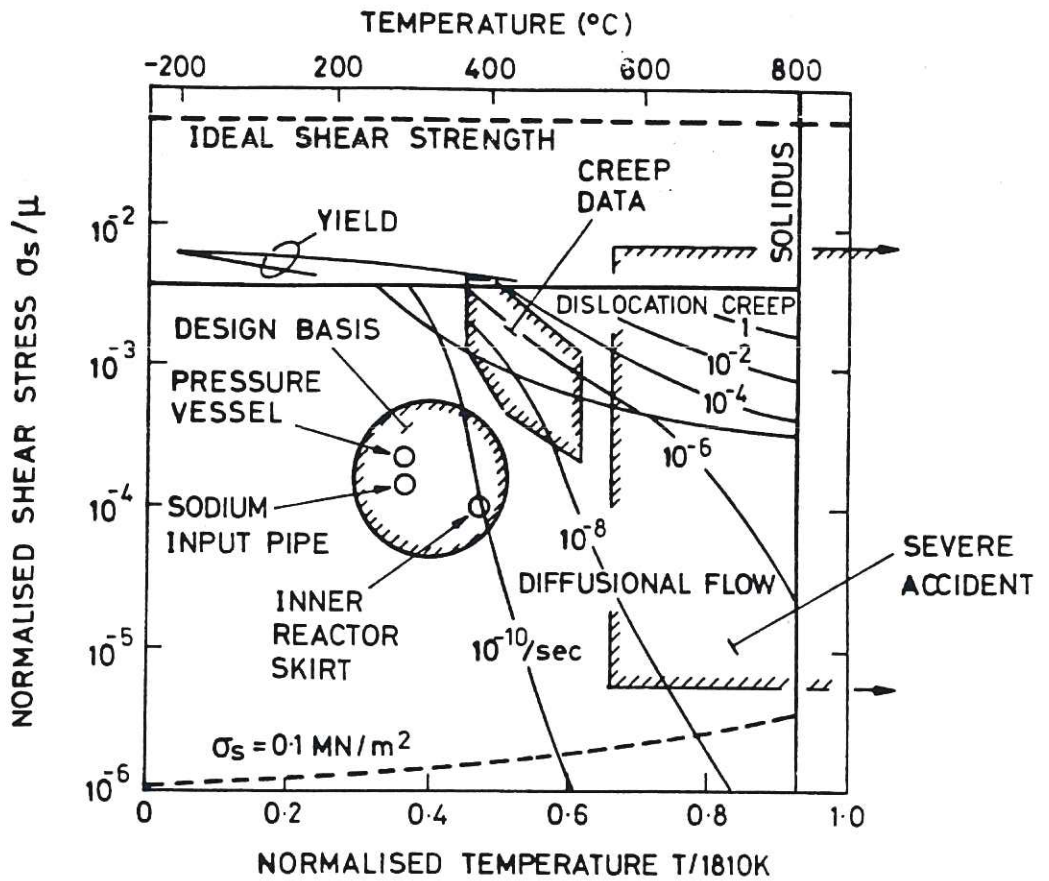
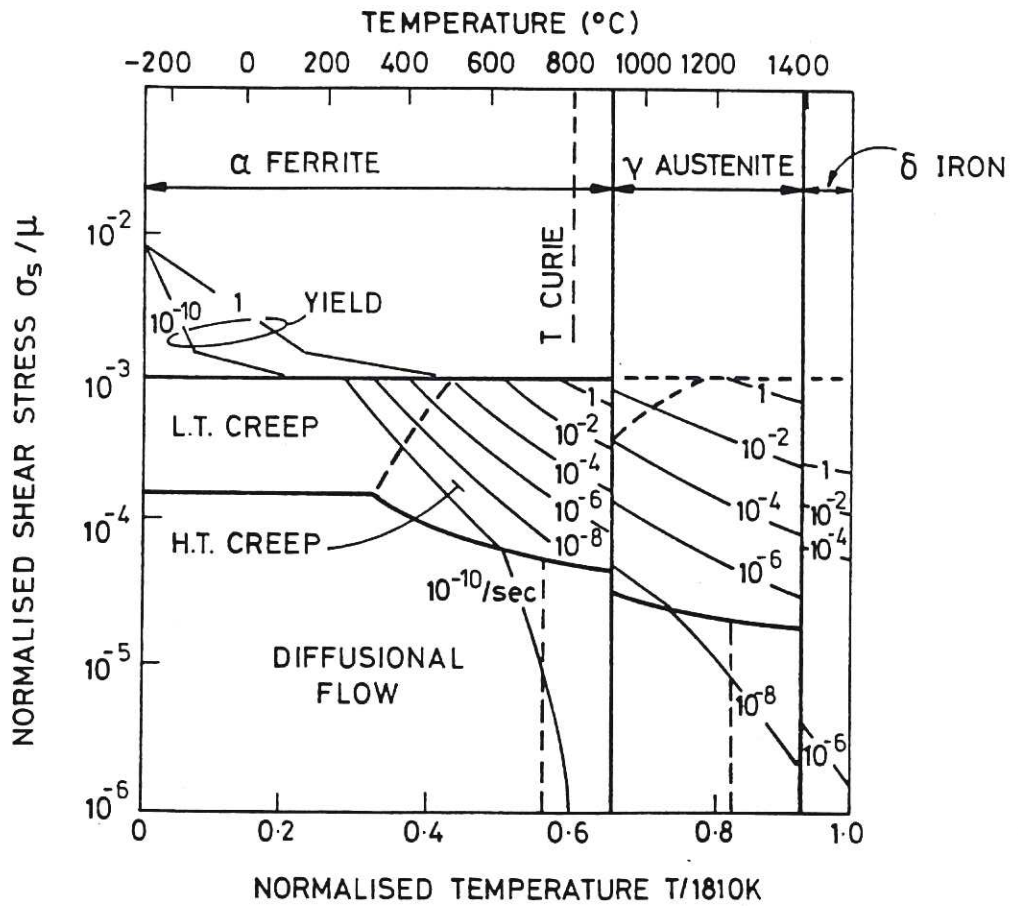


Figure 1 Failure Modes



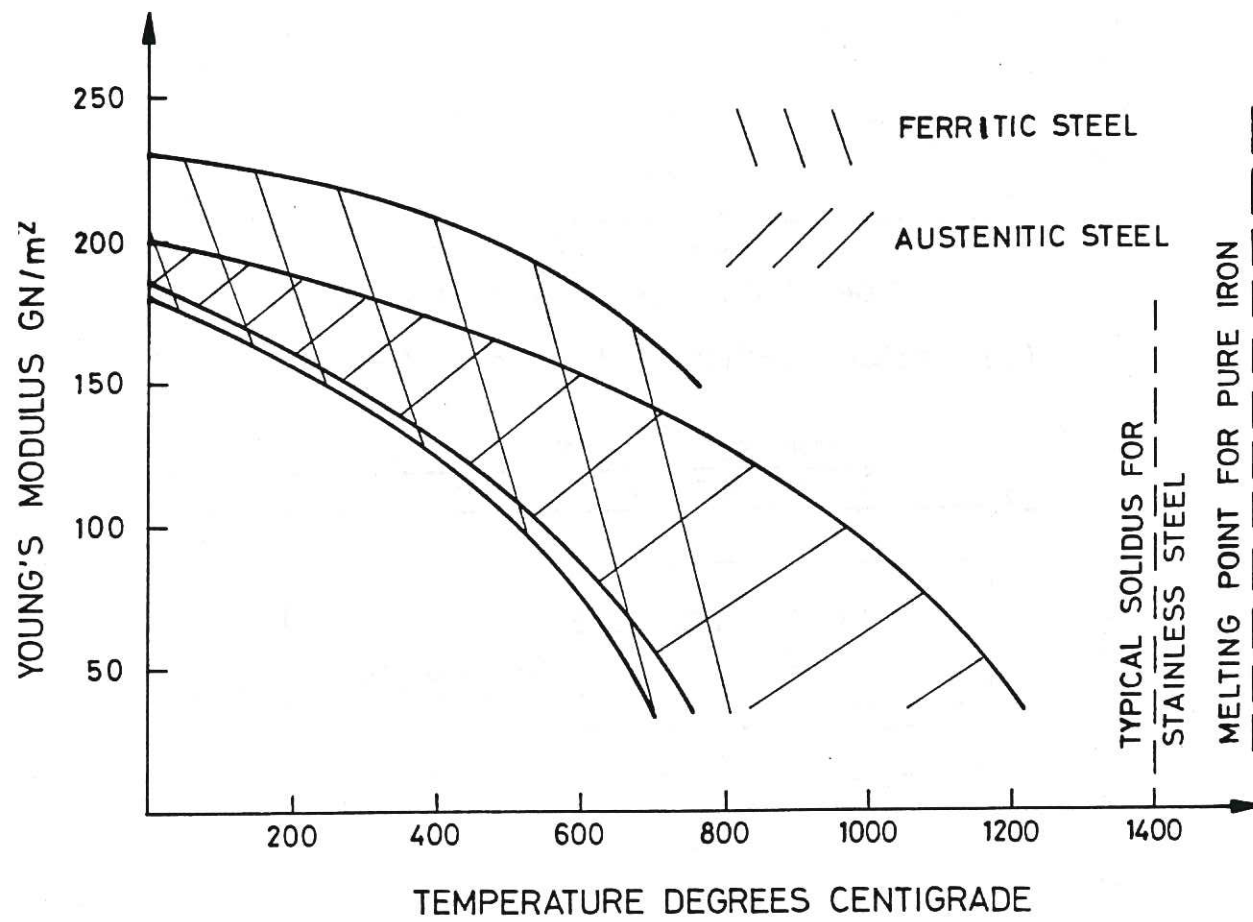
(a) Deformation Mechanism Map for 316 stainless steel. 50 μm grains.



(b) Deformation Mechanism Map for pure iron. 100 μm grains.

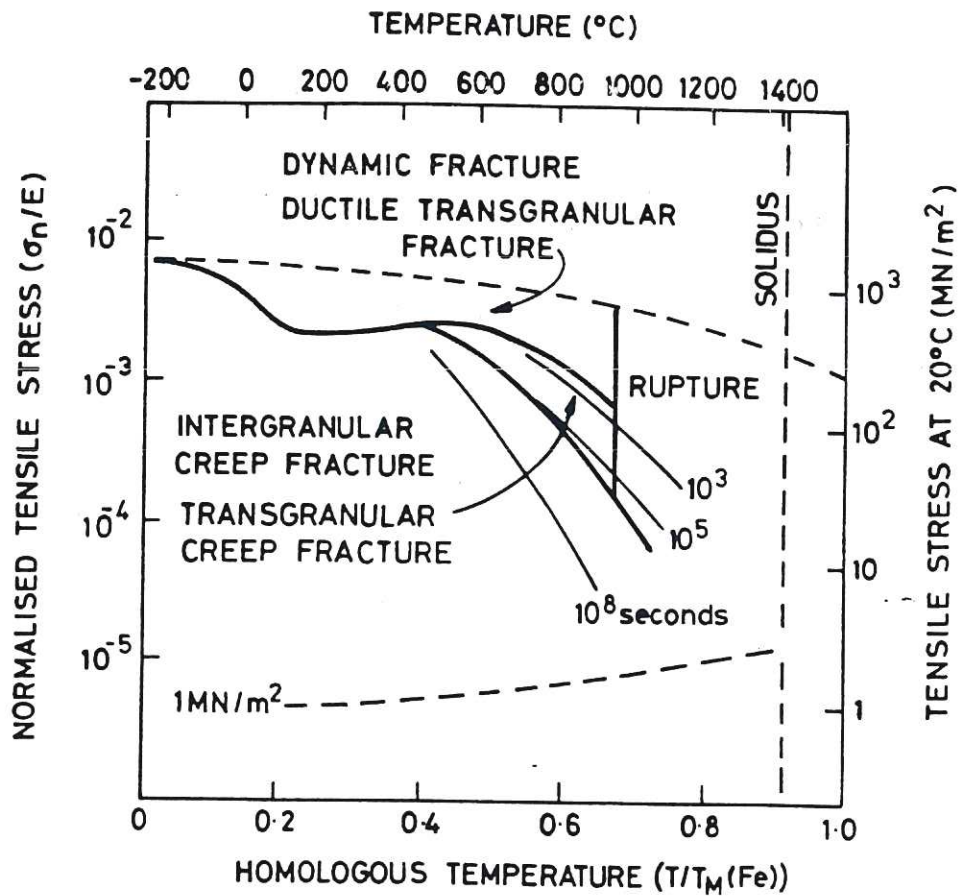
N.B. These maps are based on data from Frost and Ashby [2].

Figure 2 Deformation Mechanism Maps

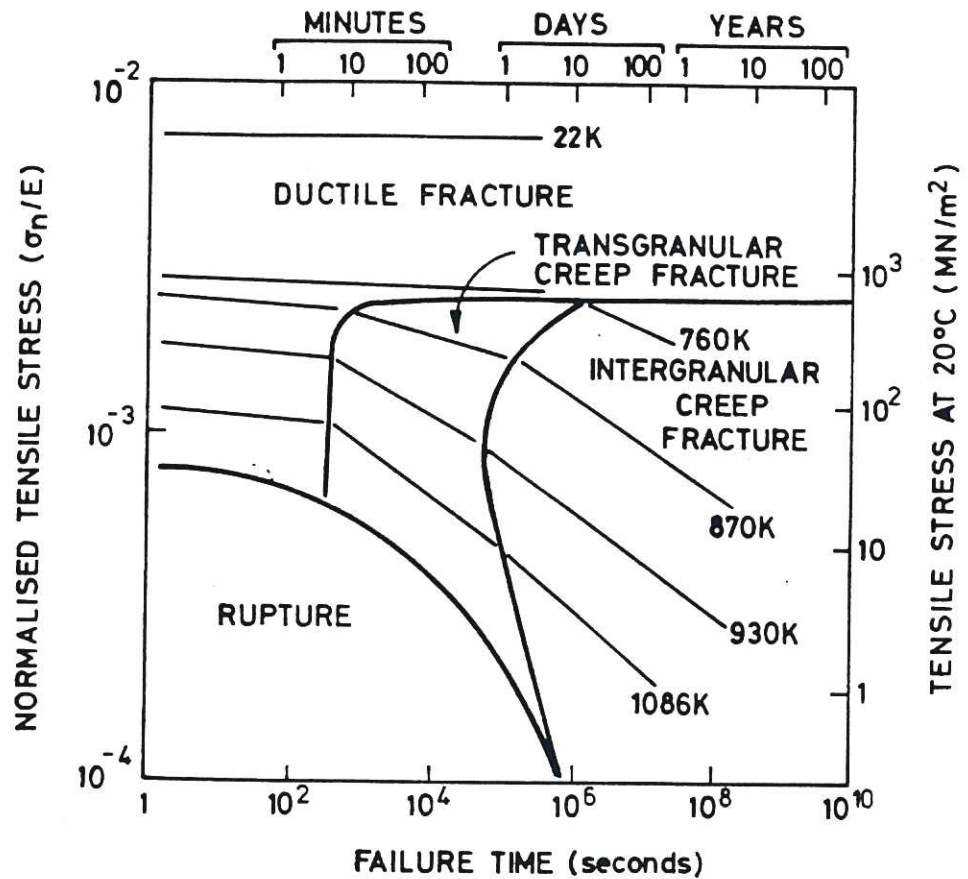


Based on data in The Fulmer Optimiser, Fulmer Research Institute 1979

Figure 3 Effect of Temperature on Young's Modulus [3]



(a) Fracture Mechanism Map for 304 stainless steel



(b) Alternative form of (a)

Based on data from Ashby, Gandhi and Taplin [4]

Figure 4 Fracture Mechanism Maps

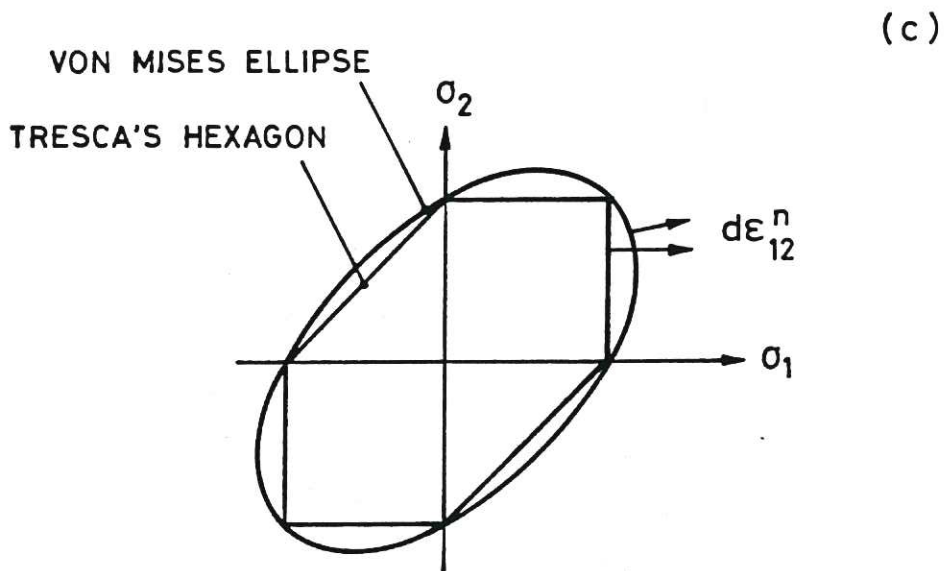
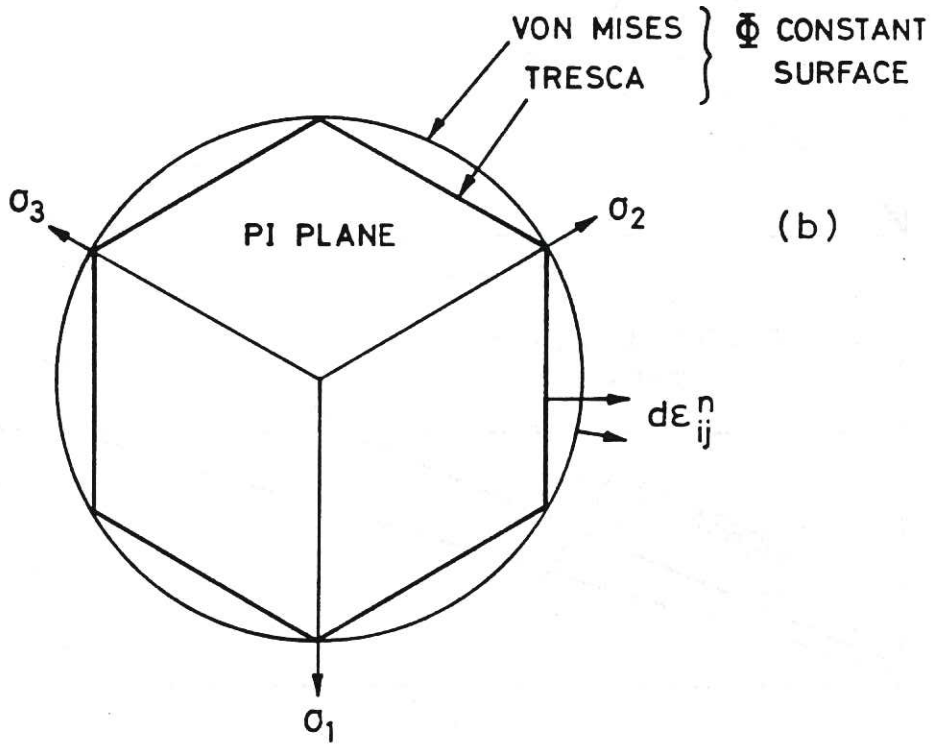
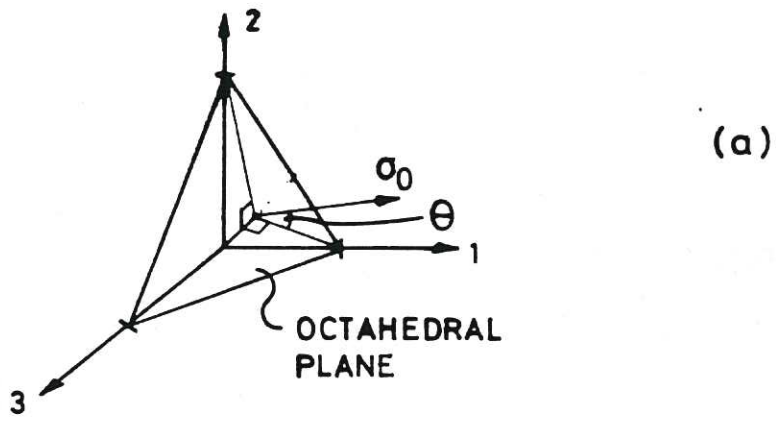


Figure 5 Non-Elastic Deformation

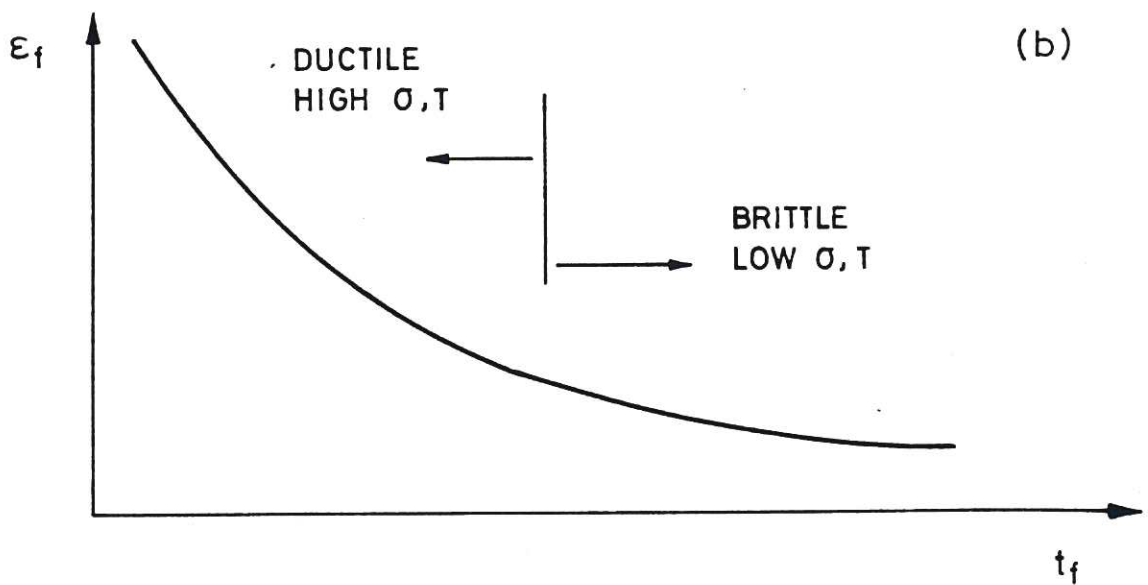
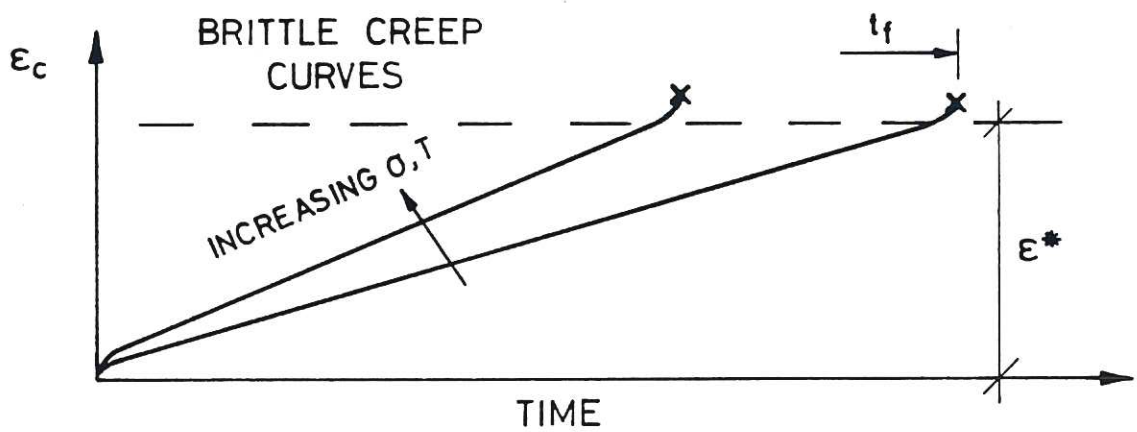
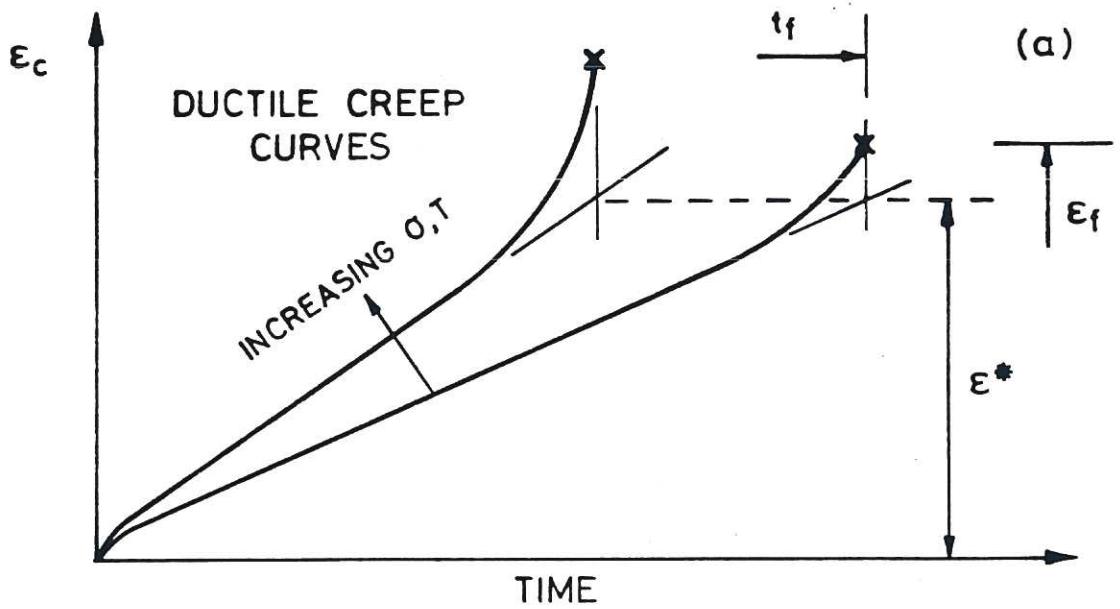
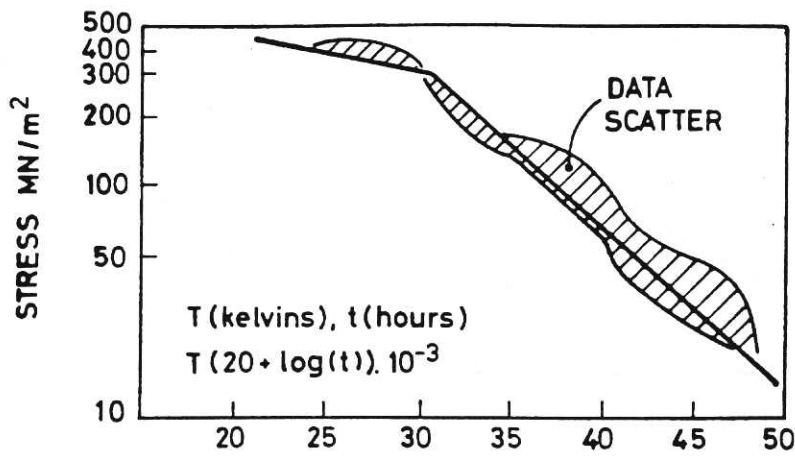
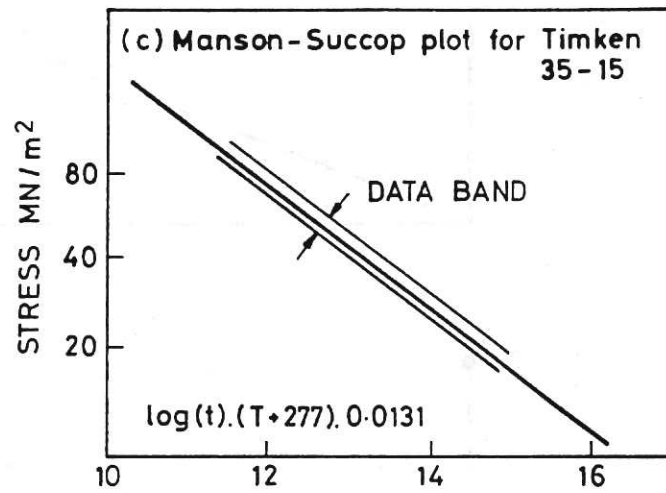
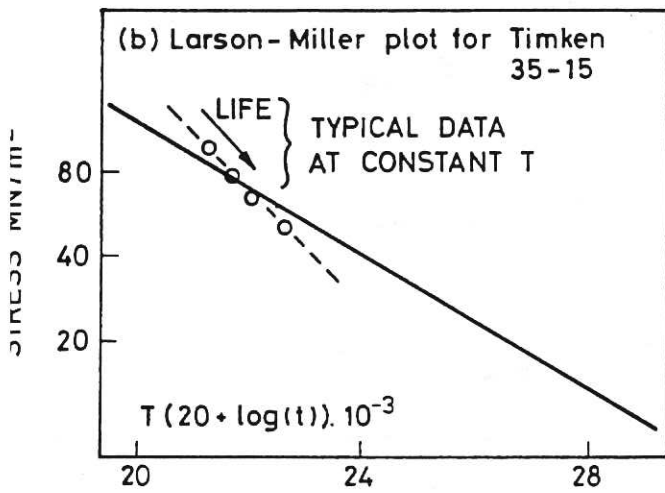


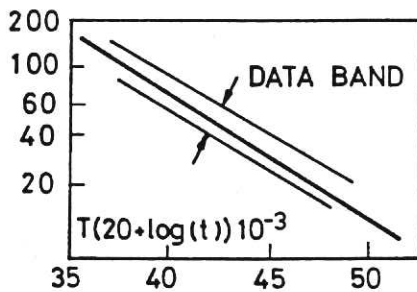
Figure 6 Creep Strain Curves



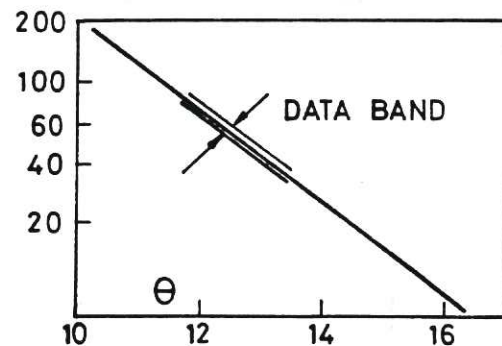
(a) Larson-Miller plot for 18-8 steel based on data from Oding [13].



N.B. (b) and (c) are based on data from Clauss [14]



(d) Larson-Miller plot for stainless steel



(e) Dorn plot for stainless steel

N.B. (d) and (e) are based on data from Rabotnov [11]

Figure 7 Empirical Methods

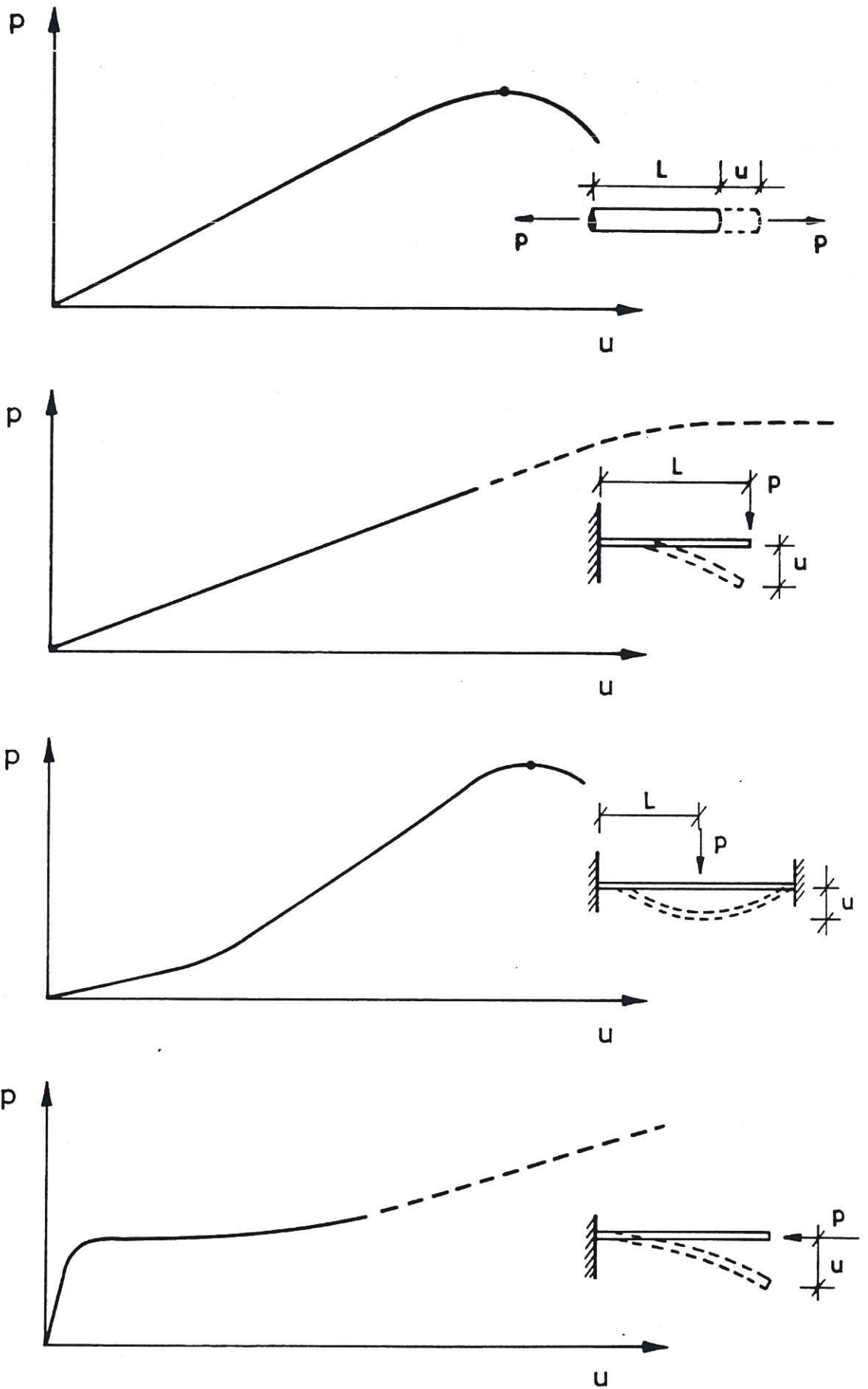


Figure 8 Large Deflection Behaviour

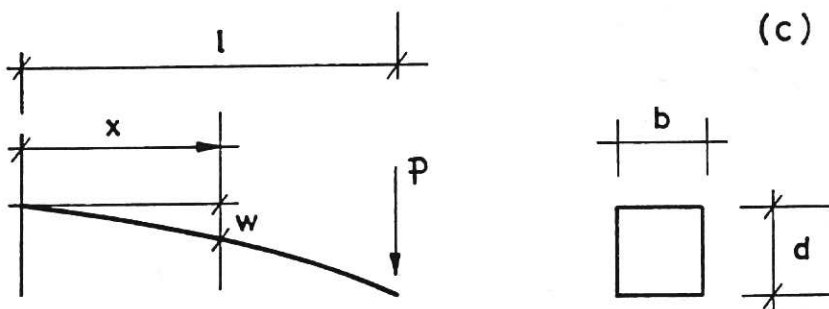
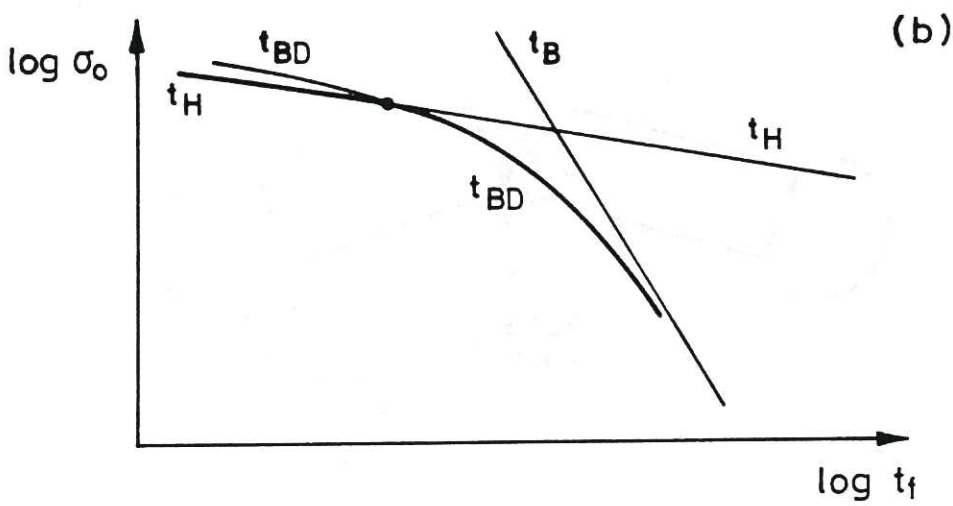
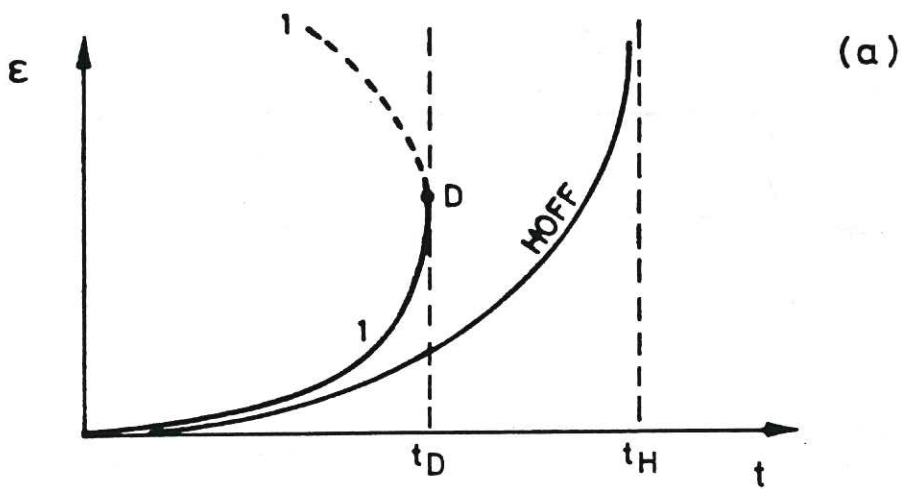
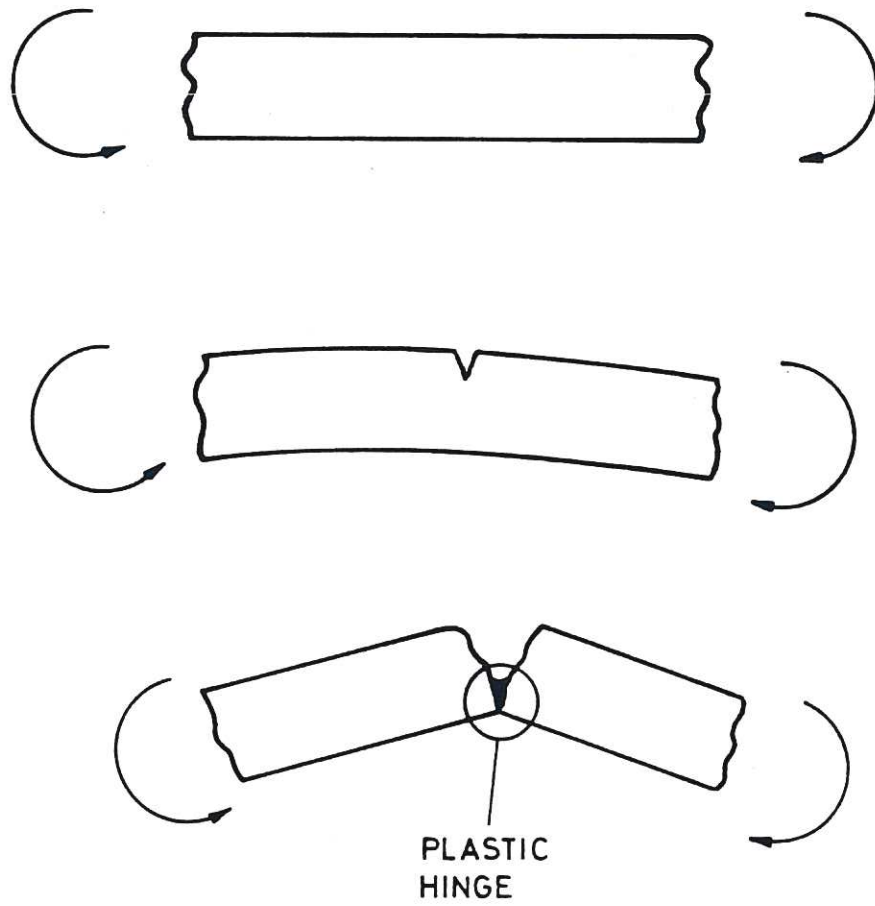


Figure 9

BRITTLE CREEP FAILURE IN BENDING

(a)



IDEAL 'I' BEAM

(b)

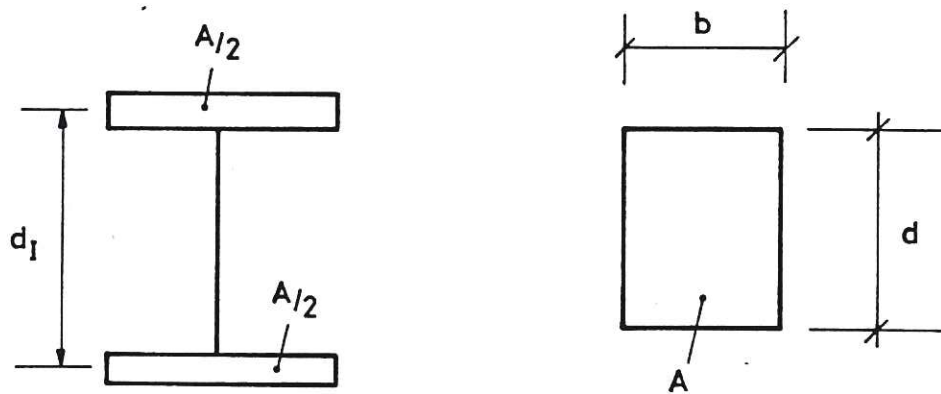


Figure 10

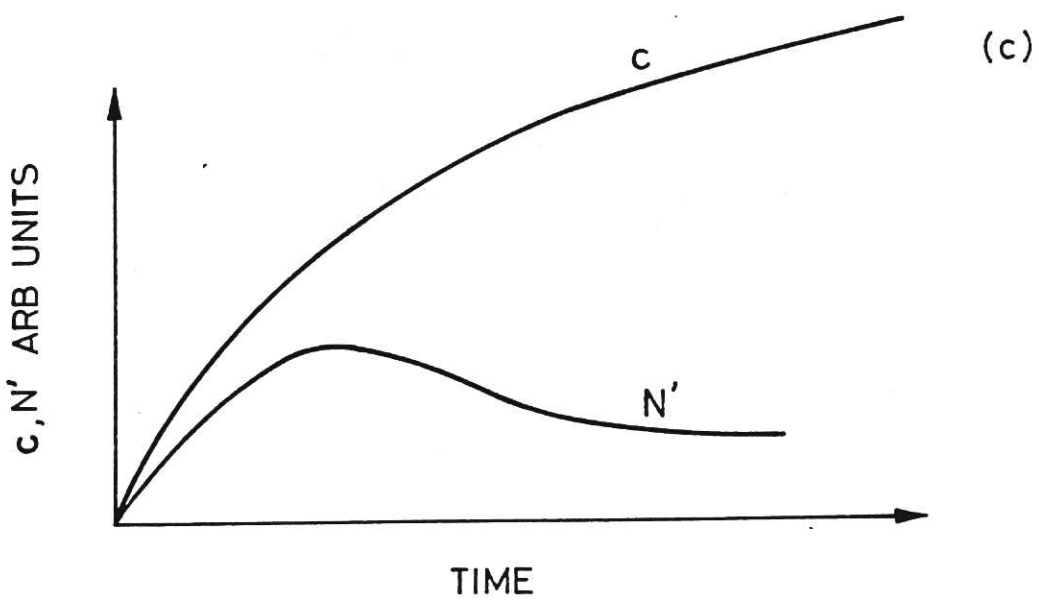
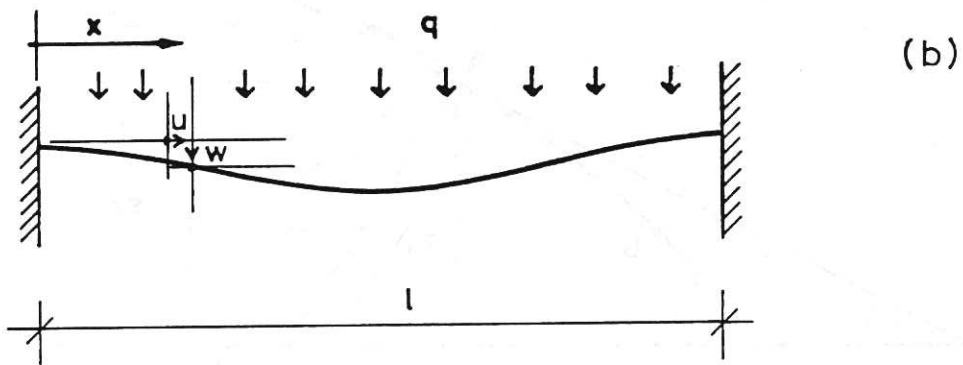
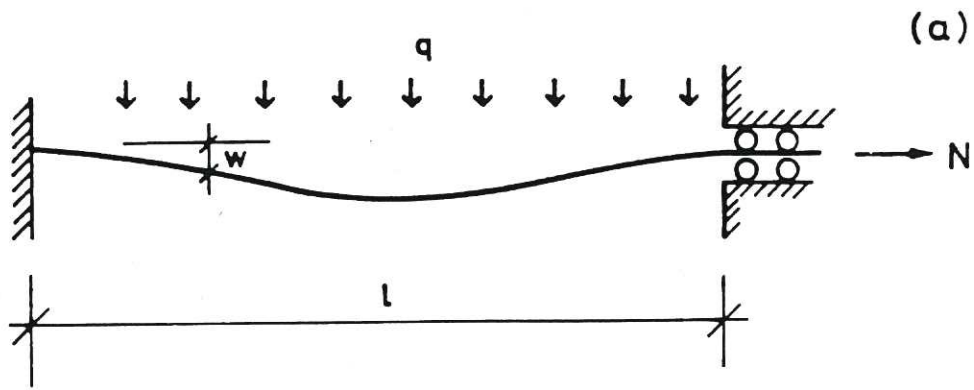


Figure 11

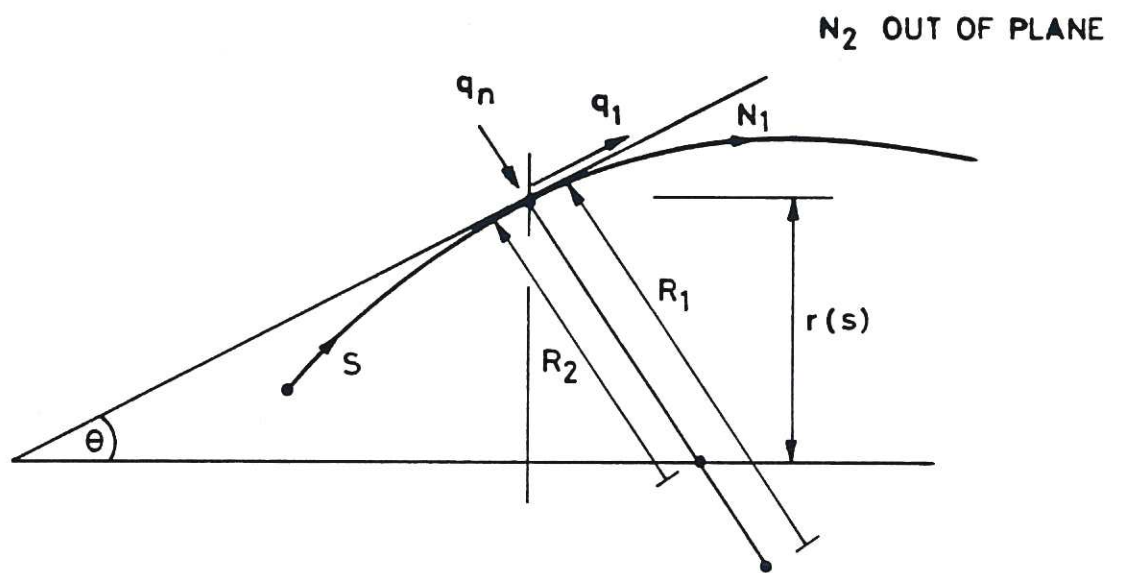


Figure 12 Axisymmetric Shell

APPENDIX 1

FAILURE OF HOMOGENEOUSLY STRESSED STRUCTURES AT HIGH TEMPERATURE

A1. INTRODUCTION

Many of the important features of structural failure at high temperature can be illustrated using idealised examples for which analytical or simple numerical solutions can be found. Here solutions have been found for structures in which the stresses and temperature are uniform in space, at least up to the onset of failure, and failure is precipitated by either ductile or brittle creep. This family of solutions covers bars in tension and thin walled spheres and cylinders under internal pressure. Where such failures are due to increasing load without creep deformation analytical solutions already exist (e.g. [A1]). Here these solutions have been extended to cover failure induced by creep deformation at constant load.

The problem is defined by:-

- (a) Structure and nature of the loads. Here this implies a statically determinate structure with homogeneous, but time dependent, stresses and temperature.
- (b) Strain displacement relationships. As large deformations and large strains are possible these must be based on natural strains (i.e. $de_i = dx_i/x_i$ etc.) rather than engineering strains (i.e. $de_i = dx_i/x_{i0}$).
- (c) Failure criteria. For ductile behaviour failure occurs when the structure becomes unstable due to the combination of material and geometrical non-linearities. For brittle behaviour the Kachanov damage model will be used [A2] to determine when the material has become sufficiently damaged by brittle creep to precipitate fracture.
- (d) Material constitutive law. This relates the strain, ϵ , to the stress, σ , and any other relevant parameters e.g. temperature, T time, t , elasticity, strain rate or previous loading history. Since we are

interested here in structures undergoing inelastic deformations slowly and monotonically, it is reasonable to use a simple constitutive law based on superposition of a time independent plastic strain, and a time dependent creep strain.

$$\text{i.e.} \quad \epsilon = \epsilon_p(\sigma, T) + \epsilon_c(\sigma, T, t) \quad (\text{A1})$$

Here we will use a power law form of the plastic strain and the Dorn equation [A3] for creep strain. Thus:-

$$\epsilon = (\sigma/\sigma_p)^m + \int_0^t (\sigma/\sigma_c)^n \exp(-Q/RT) dt \quad (\text{A2})$$

where R is the universal gas constant and σ_p , σ_c , Q, m, and n are material properties. Here we are interested in bi-axial as well as uniaxial stress systems which for non-elastic deformation involves defining a significant stress and a significant strain, which can be used to relate plastic and creep deformation in multiaxially stressed structures to uniaxial stress and strain measurements. The Von Mises criterion will be used here.

A2. ANALYTICAL SOLUTION FOR DUCTILE CASE

The Von Mises significant stress, σ , and strain increment, $d\epsilon$, are given by [A1]:-

$$\sigma = [\frac{1}{2}(\sigma_1 - \sigma_2)^2 + \frac{1}{2}(\sigma_2 - \sigma_3)^2 + \frac{1}{2}(\sigma_1 - \sigma_3)^2]^{\frac{1}{2}} \quad (\text{A3})$$

$$d\epsilon = [\frac{2}{9} (d\epsilon_1 - d\epsilon_2)^2 + \frac{2}{9} (d\epsilon_2 - d\epsilon_3)^2 + \frac{2}{9} (d\epsilon_1 - d\epsilon_3)^2]^{\frac{1}{2}} \quad (\text{A4})$$

and the associated flow rule which determines the strain increment direction is given by:-

$$(2\sigma_1 - \sigma_2 - \sigma_3)/d\epsilon_1 = (2\sigma_2 - \sigma_1 - \sigma_3)/d\epsilon_2 = (2\sigma_3 - \sigma_1 - \sigma_2)/d\epsilon_3 \quad (\text{A5, A6})$$

where σ_1 , $d\epsilon_1$ etc. are the principal stresses and strain increments respectively. For further details of this see section 3.1 in the main report.

Consider the case of a thin walled sphere of radius r , thickness h , under internal pressure p , in which directions 1 and 2 are in the sphere surface and direction 3 is radial, then equilibrium requires that:-

$$\sigma_1 = \sigma_2 = \frac{pr}{2h} \quad \sigma_3 = 0 \quad (\text{A7, A8, A9})$$

The strain displacement relationships here are:-

$$d\epsilon_1 = d\epsilon_2 = \frac{dr}{r} \quad \text{and} \quad d\epsilon_3 = \frac{dh}{h} \quad (\text{A10, A11, A12})$$

From (A5-A9) it follows that $d\epsilon_3 = -2d\epsilon_1$ and hence from (A3) and (A4) $\sigma = \sigma_1$ and $d\epsilon = 2d\epsilon_1$.

$$\text{From (A7)} \quad \frac{dp}{p} = \frac{d\sigma_1}{\sigma_1} + \frac{dh}{h} - \frac{dr}{r} \quad (\text{A13})$$

$$\text{Hence} \quad \frac{dp}{p} = \frac{d\sigma}{\sigma} - \frac{3}{2} d\epsilon \quad (\text{A14})$$

$$\text{and integrating} \quad \sigma = [\exp(\frac{3}{2} (\epsilon - \epsilon_0))] \sigma_0 p / p_0 \quad (\text{A15})$$

where subscript 0 denotes initial or reference value.

Equations (A14) and (A15) relate the stress, strain and load which will yield a solution when either stress or strain is eliminated using the constitutive law.

The analysis of the bar and cylinder are analogous and all the solutions up to this stage are summarised in table A1 and can be expressed by:-

$$\sigma = [\exp(\gamma_c (\epsilon - \epsilon_0))] \sigma_0 p / p_0 \quad (\text{A16})$$

where γ_c the 'critical subtangent' is a structure dependent constant (given in table A1). The creep independent increasing load solution can be readily derived from (A16) since failure will occur when the maximum pressure is reached i.e. when $dp = 0$ or (noting $\epsilon_0 = 0$ here):-

$$\frac{1}{\sigma} \frac{d\sigma}{d\epsilon} \equiv \gamma \leq \gamma_c \quad (\text{A17})$$

The subtangent γ is a strain dependent material property and for a power law plastic strain assumption the point of instability is given by:-

$$\gamma = \gamma_c \quad \epsilon_p = 1/m\gamma_c \quad \sigma = \sigma_p (m\gamma_c)^{-1/m} \quad (\text{A18, A19, A20})$$

and
$$p = l_c \sigma_p (e m \gamma_c)^{-1/m} \text{ where } e = 2.71828\dots \quad (\text{A21})$$

l_c is a structure dependent constant (see table A1). Note that for the bar case p should be replaced by L/A_0 where L is the axial load and A_0 the initial cross-sectional area of the bar.

Failure due to ductile creep deformation

We now consider the case of a structure loaded initially to less than critical conditions but then allowed to deform at constant load due to creep. For simplicity at this stage a linear temperature variation with time will be assumed. The definition of ductile instability requires to be extended now since variation with time must be considered [A2] i.e. instability occurs when either:-

$$\frac{dF}{du} = 0 \quad \text{or} \quad \frac{dt}{du} = 0 \quad (\text{A22, A23})$$

where F , u and t represent load, displacement and time respectively. In the creep independent case instability was reached when (A22) was satisfied but in the creep case (A22) is always satisfied since we have defined $dF = 0$ (and $du \neq 0$) and instability will now occur when (A23) is satisfied. This in effect means that the structure passes through an extended neutral equilibrium until (A23) is satisfied. Thus instability occurs when $dt/du=0$ or here $\dot{\epsilon}, \dot{\sigma} \rightarrow \infty$ where ($\dot{}$) denotes time derivative. Differentiating the constitutive law assuming temperature independent plastic properties (the more realistic case where σ_p is allowed to vary with temperature is discussed below) gives:-

$$\dot{\epsilon} = m \left(\frac{\sigma}{\sigma_p}\right)^m \frac{\dot{\sigma}}{\sigma} + \left(\frac{\sigma}{\sigma_c}\right)^n \exp(-Q/RT) \quad (\text{A24})$$

and the time derivative of (A16) gives:-

$$\dot{\sigma} = \gamma_c \dot{\epsilon} \sigma_o \exp(\gamma_c(\epsilon - \epsilon_o)) \quad (A25)$$

From (A24) and (A25)

$$\dot{\epsilon} [\exp(-n\gamma_c(\epsilon - \epsilon_o)) - m\epsilon_o\gamma_c \exp(\gamma_c(\epsilon - \epsilon_o)(m-n))] = \left(\frac{\sigma_o}{\sigma_c}\right)^n \exp(-Q/RT) \quad (A26)$$

$$\text{Thus} \quad \dot{\epsilon} \rightarrow \infty \text{ when } \epsilon - \epsilon_o = \epsilon_o - (m\gamma_c)^{-1} \ln(m\gamma_c \epsilon_o) \quad (A27)$$

For a linear temperature variation $T = T_o + \beta t$ equation (A26) can be integrated from ϵ_o, T_o to ϵ_I, T noting that

$$\int_0^t \exp(-Q/RT) dt = \beta^{-1} \int_{T_o}^T \exp(-Q/RT) dT = T\beta^{-1} E_2(Q/RT) - T_o\beta^{-1} E_2(Q/RT_o) \quad (A28)$$

where $E_2(Z)$ is the exponential integral function $-\int t^{-2} \exp(-Zs) ds$. The solution is then given by

$$g(Q/RT) = f(\epsilon_o) \quad (A29)$$

$$\text{where} \quad g(Q/RT) = \left(\frac{\sigma_p}{\sigma_c}\right)^n \beta^{-1} [T E_2(Q/RT) - T_o E_2(Q/RT_o)] \quad (A30)$$

$$\text{and} \quad f(\epsilon_o) = \epsilon_o^{-n/m} \left[\frac{1}{n\gamma_c} (1 - (m\gamma_c \epsilon_o)^{n/m}) + \frac{m\epsilon_o}{m-n} (1 - (m\gamma_c \epsilon_o)^{\frac{n-m}{m}}) \right] \quad (A31)$$

For the constant temperature case $\beta \rightarrow 0$ and (A30) reduces to

$$g(Q/RT) = t \left(\frac{\sigma_p}{\sigma_c}\right)^n \exp(-Q/RT_o) \quad (A32)$$

Thus given the material constants and the initial strain ϵ_o , $f(\epsilon_o)$ can be evaluated from (A31) and solutions found for the temperature when the instability occurs using (A29, A30) for finite heating rates, or the time when the instability occurs using (A29, A32) for the constant temperature case. For cases of interest here $Q/RT \gg 1$ and the exponential integral function can be approximated:-

$$\text{i.e.} \quad E_2(Z) = \frac{1}{2+Z} \exp(-Z) \text{ for large } Z \text{ (error } < 1\% \text{ for } Z > 10) \quad (A33)$$

The functions $g(Q/RT)$ and $f(\epsilon_0)$ are illustrated in figure A1 for the case of a sphere ($\gamma_c = 1.5$) with $T_0 = 0$ and with materials data based on type 304 stainless steel for which the following have been taken:- $Q = 279.6$ kJ/mole ($R = 8.314 \times 10^{-3}$ J/mole K), $\sigma_p = 223$ MN/m², $n = 7.5$, $m = 6.75$ and $T = 1680$ K. Note that the variation of σ_p with temperature has been ignored at this stage and the single value at $T = 0.75 T_m$ used instead.

From these, failure maps have been produced of initial strain versus temperature for the $\beta = 0$ case and initial strain versus normalised heating rate, $\beta R/Q$, for the case $T_0 = 0$ (figure A2). In both cases a creep induced failure zone is bounded by instant plastic instability for large initial strain, and by melting for large initial temperature or large heating rate.

Temperature dependent plastic properties

Above it was assumed that the plastic properties were temperature independent which is not realistic for most materials. The more practical case where m is temperature independent but $\sigma_p = \sigma_p(T)$ is considered below. Equation (A24) now becomes:-

$$\dot{\epsilon} = m \left(\frac{\sigma}{\sigma_p}\right)^m \frac{\dot{\sigma}}{\sigma} + \left(\frac{\sigma}{\sigma_c}\right)^n \exp(-Q/RT) - \frac{m}{\sigma} \left(\frac{\sigma}{\sigma_p}\right)^{m+1} \frac{d\sigma_p}{dT} \frac{dT}{dt} \quad (A34)$$

then substituting the previous expressions for σ and $\dot{\sigma}$ which are not affected by σ_p (equations (A16) and (A25) we obtain

$$\dot{\epsilon} = \frac{\left(\frac{\sigma_0}{\sigma_c}\right)^n \exp[(n-m)\gamma_c (\epsilon - \epsilon_0) - Q/RT] - \frac{m}{\sigma_p} \left(\frac{\sigma_0}{\sigma_p}\right)^m \frac{d\sigma_p}{dT} \frac{dT}{dt}}{\exp(-m\gamma_c (\epsilon - \epsilon_0)) - m\gamma_c \left(\frac{\sigma_0}{\sigma_p}\right)^m} \quad (A35)$$

This can be integrated numerically to give $\epsilon(t)$ for arbitrary $\sigma_p(T)$ and dT/dt once $T(t)$ has been specified. This equation is valid provided $\dot{\epsilon} > 0$ and the instability occurs when $\dot{\epsilon} \rightarrow \infty$.

i.e. when
$$\epsilon = \epsilon_I = -\frac{1}{m\gamma_c} \ln[m\gamma_c \left(\frac{\sigma_0}{\sigma_p}\right)^m] + \epsilon_0 \quad (A36)$$

Normally $d\sigma_p/dT < 0$ and ϵ_I will fall with temperature.

A3. Brittle Creep Case

In the analysis above it has been assumed that the material possesses infinite ductility since no restriction was placed on the strain accumulated before the instability occurred. However failure may occur prior to this instability due to loss of ductility. This creep induced embrittlement occurs in most materials after prolonged exposure to stress at high temperature and is commonly due to accumulation of internal voids caused by vacancies diffusing to grain boundaries. If severe enough these voids coalesce and cause complete failure characterised by an intergranular fracture surface. It is assumed that this process is independent of ductile creep which involves movement within the grains. A means of analysing this behaviour was formulated by Kachanov [A2] who introduced a damage factor, D , where

$$D = (A - A_r)/A \quad \text{and} \quad \frac{dD}{dt} = \left[\frac{\sigma}{\sigma_k (1-D)} \right]^v \frac{1}{t_k (1+v)} \quad (\text{A37, A38})$$

where the material cross-sectional area, or thickness, A is reduced to A_r by internal void formation. σ_k and v are material constants. Note that the stress, σ , is still based on the area A . Failure occurs at $t = t_{BD}$ when $D=1$ and this is given by:-

$$\int_0^1 (1-D)^v dD = \frac{1}{1+v} = \int_0^{t_{BD}} \left(\frac{\sigma}{\sigma_k} \right)^v \frac{dt}{t_k (1+v)} \quad (\text{A39})$$

If the brittle failure time t_{BD} is less than that for ductile failure t_D (evaluated from the condition $\epsilon - \epsilon_I$ in section A2) then the failure time is t_{BD} . Otherwise the failure is ductile and t_D gives the failure time.

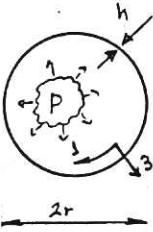
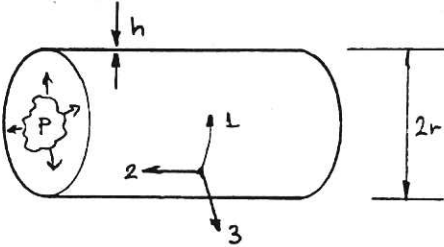
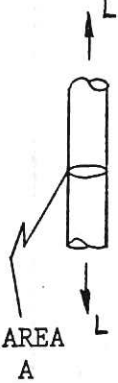
The right hand side of (A39) can be evaluated as a function of time using the expression for σ from equation (A16) and the value of strain ϵ for the general case from the numerical integration of equation (A35). A method of doing this is described in [A4].

Note that σ_k varies with temperature for most materials and this can be included in a numerical integration of equation (A39).

4. REFERENCES FOR APPENDIX

- [A1] Mc.Clintock F.A. and Argon A.S., Mechanical Behaviour of Materials. Addison Wesley 1966.
- [A2] Odqvist F.K.G., Mathematical Theory of Creep and Creep Rupture. Oxford Clarendon Press 1966.
- [A3] Orr R.L., Sherby O.D. and Dorn J.E. Trans A S M 46(1954) 113.
- [A4] Upson C.J., Calculations of High Temperature Failure of Homogeneously Stressed Structures, Culham internal report 1987.

Table A1
SUMMARY OF STRUCTURAL PARAMETERS

	SPHERE	CYLINDER		BAR
				
		ZERO END LOAD	HYDROSTATIC END LOAD	
σ_1	$pr/2h$	pr/h	pr/h	L/A
σ_1/σ	1	1	$2/\sqrt{3}$	1
σ_2/σ	1	0	$1/\sqrt{3}$	0
σ_3/σ	0	0	0	0
$d\epsilon_1/d\epsilon$	$\frac{1}{2}$	1	$\sqrt{3}/2$	1
$d\epsilon_2/d\epsilon$	$\frac{1}{2}$	$-\frac{1}{2}$	0	$-\frac{1}{2}$
$d\epsilon_3/d\epsilon$	-1	$-\frac{1}{2}$	$-\sqrt{3}/2$	$-\frac{1}{2}$
γ_c	$3/2$	$3/2$	$\sqrt{3}$	1
l_c	$2h_o/r_o$	h_o/r_o	$2h_o/\sqrt{3}r_o$	1

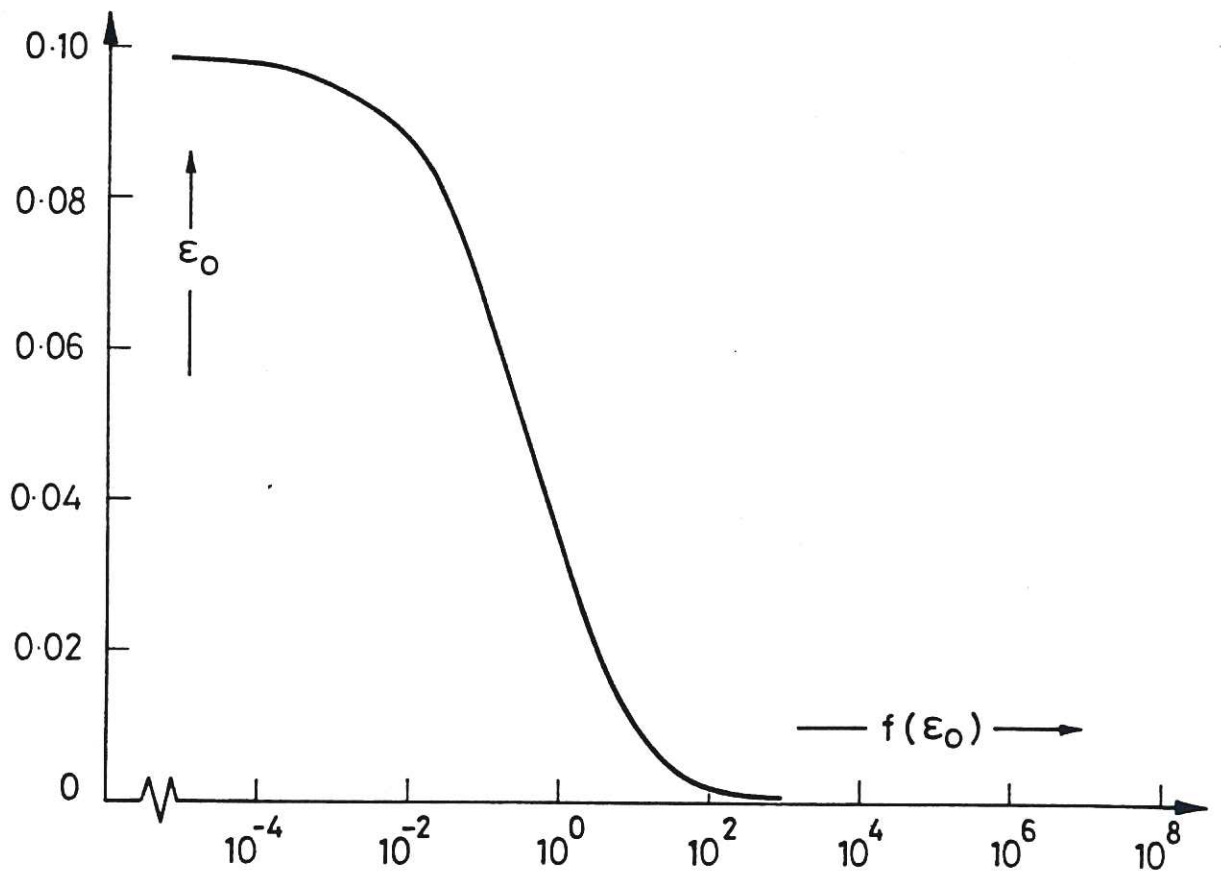
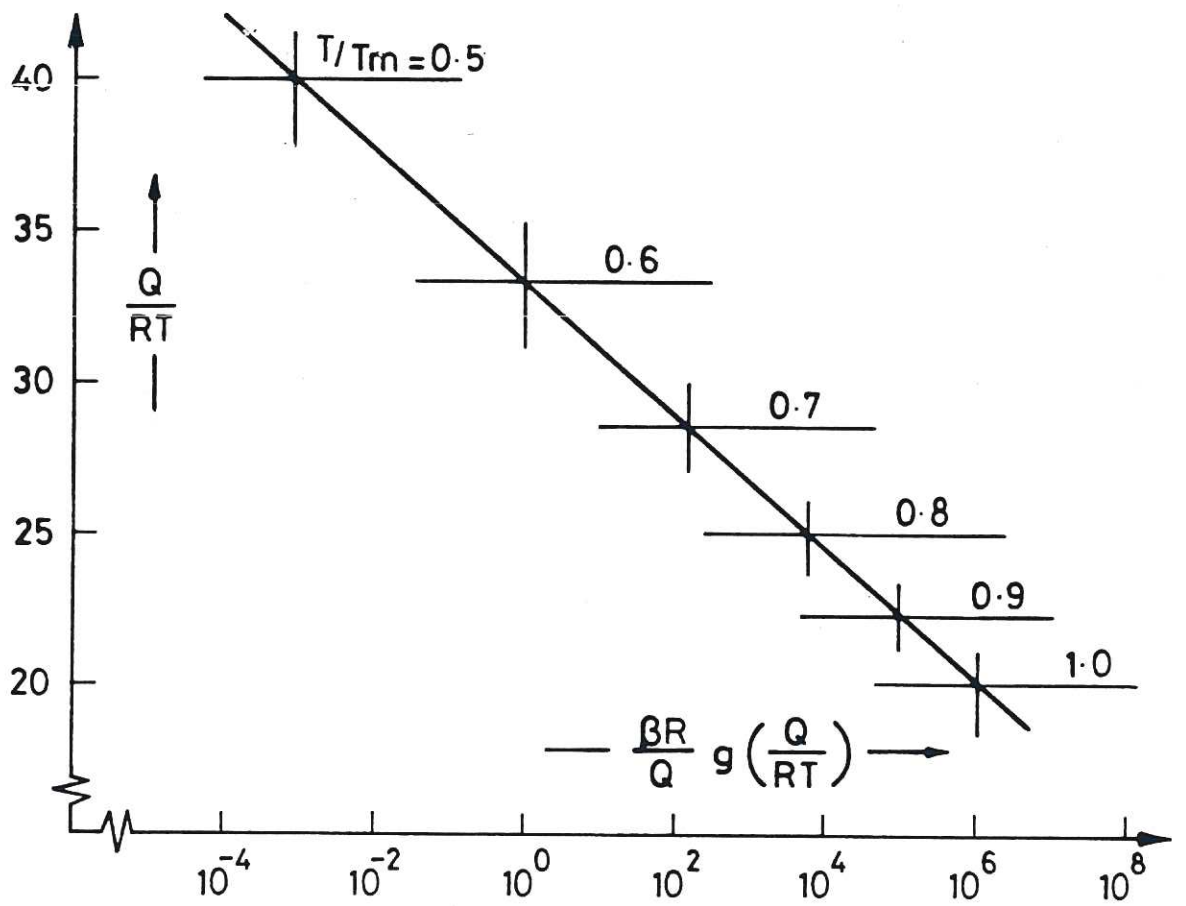


Figure A1 $f(\epsilon_0)$ and $g(Q/RT)$ for 304 S/S

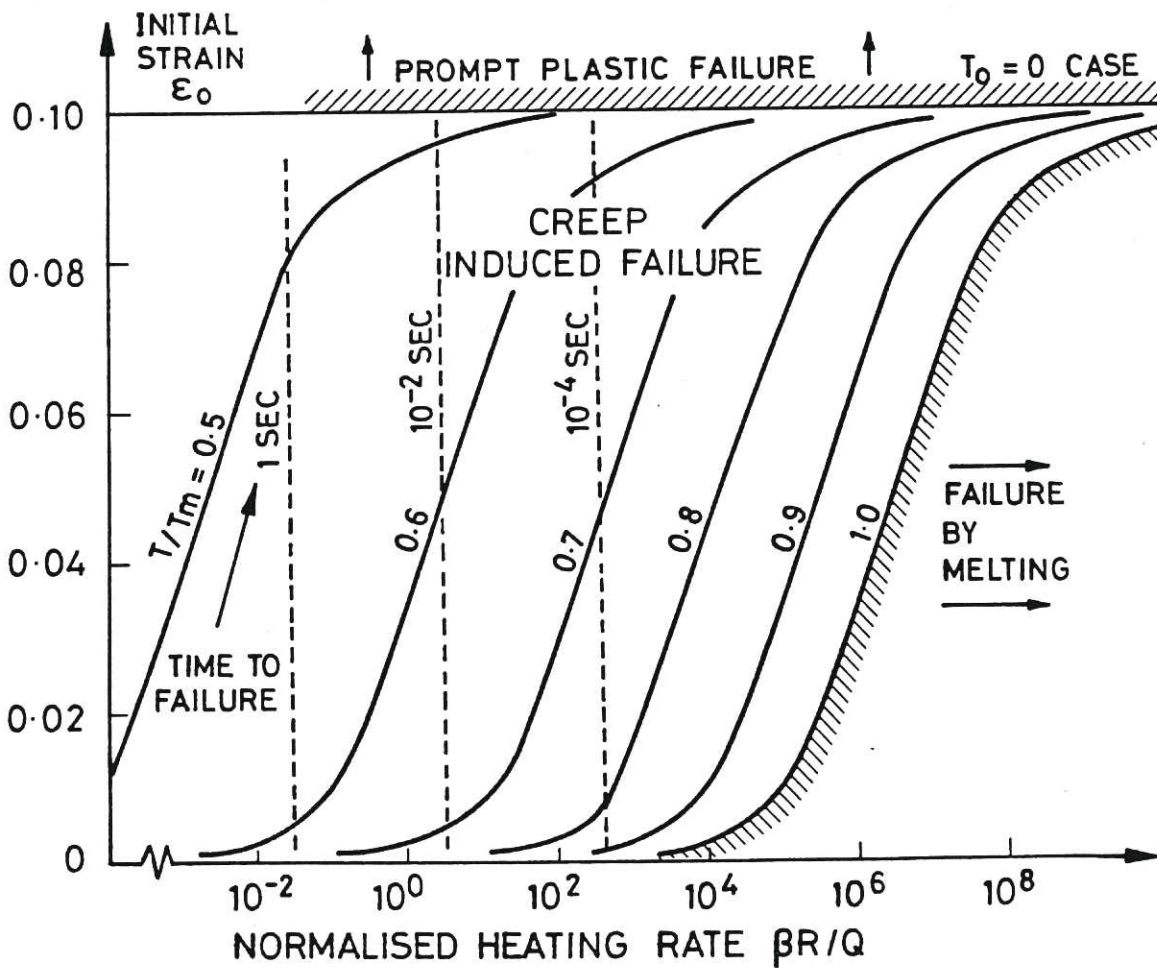
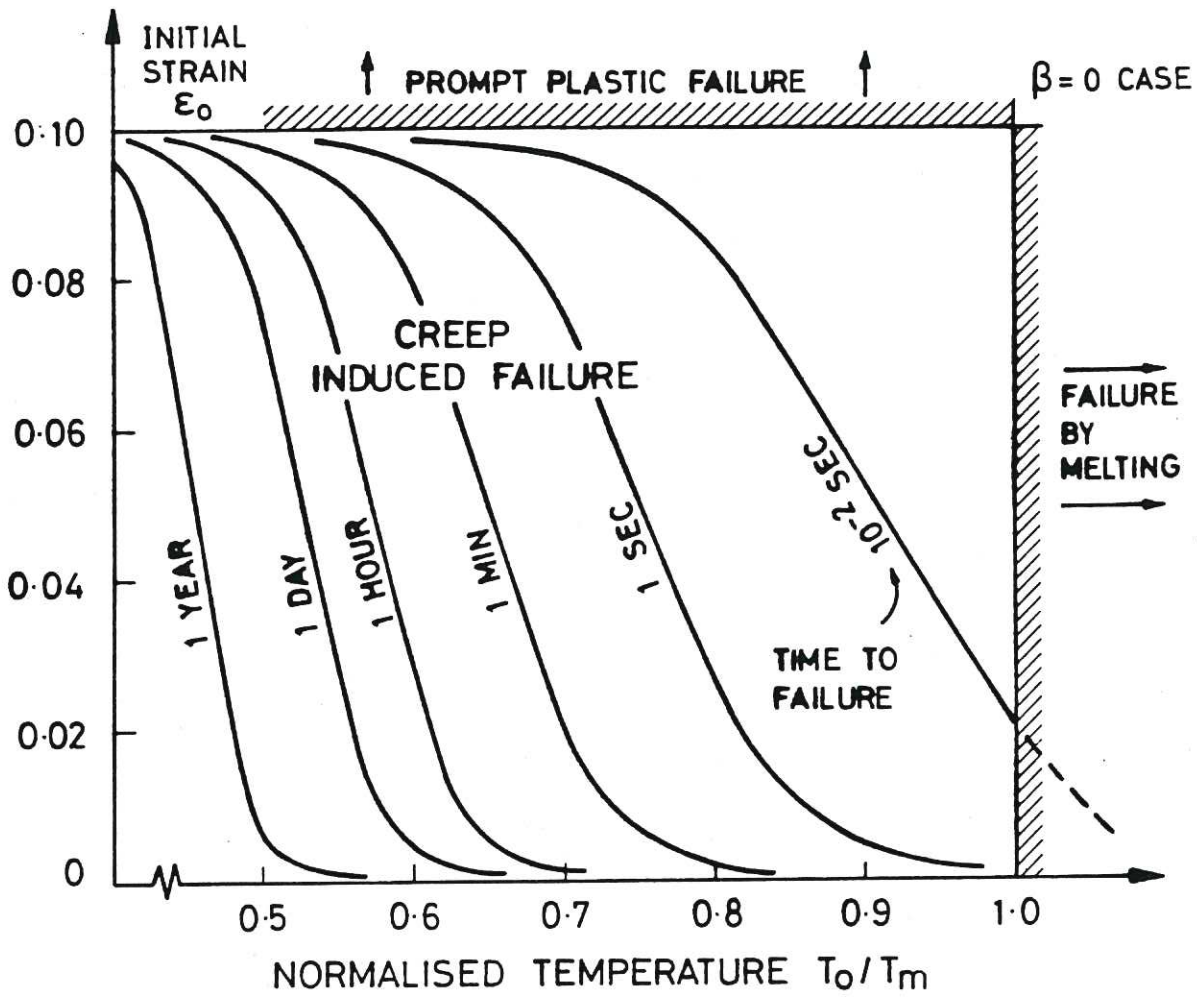
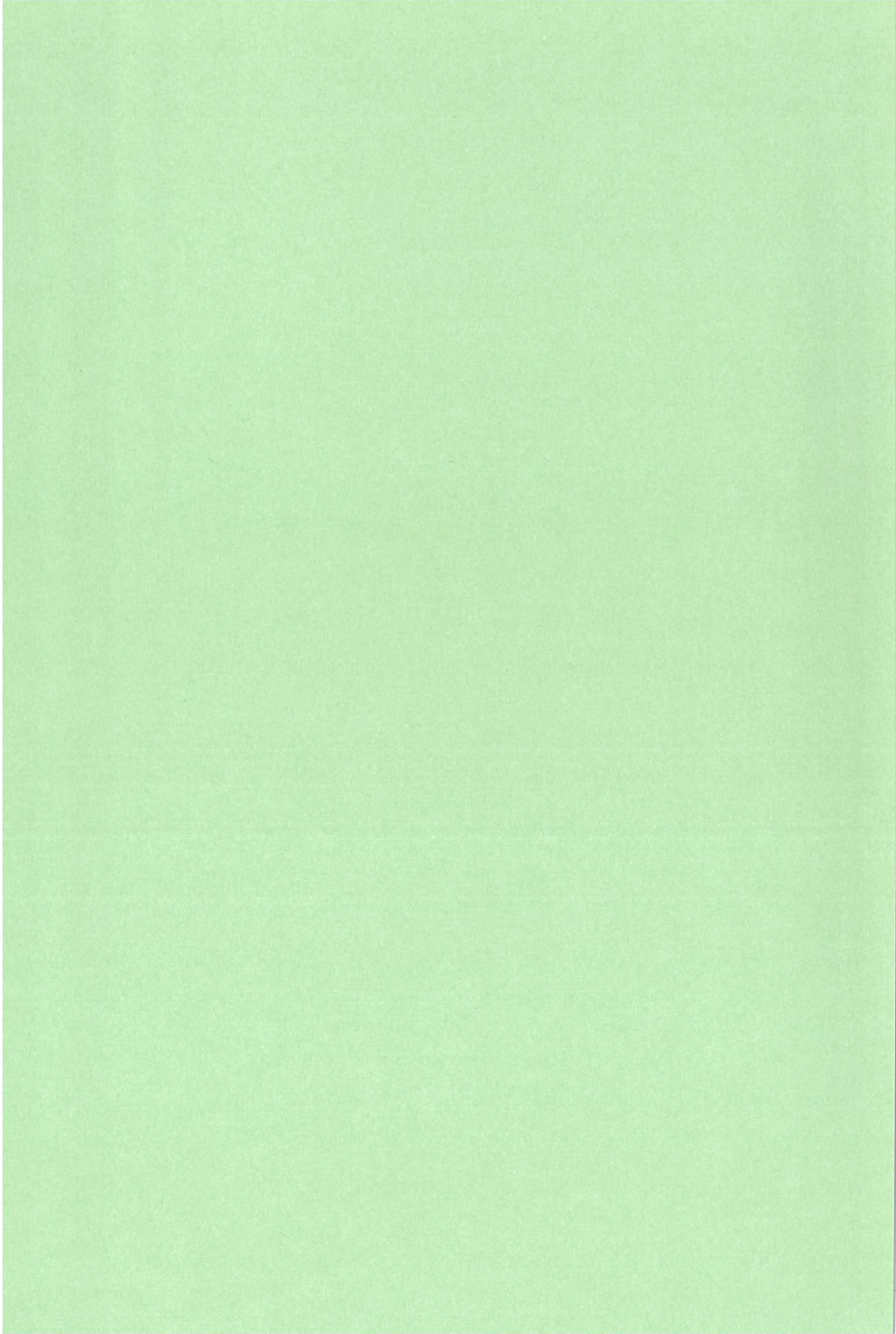


Figure A2 Failure Modes for Heated Sphere



Available, price £12.00 from:

HMSO Publications Centre

(Mail and telephone orders only)

PO Box 276, London SW8 5DT

Telephone orders 01-873 9090

General enquiries 01-873 0011

Enquiries about previously placed orders 01-873 0022

(queuing system in operation for all numbers)

HMSO Bookshops

49 High Holborn, London WC1V 6HB 01-873 0011 *(Counter service only)*

258 Broad Street, Birmingham B1 2HE 021-643 3740

Southey House, 33 Wine Street, Bristol BS1 2BQ 0272-264306

9-21 Princess Street, Manchester M60 8AS 061-834 7201

80 Chichester Street, Belfast BT1 4JY 0232-238451

71 Lothian Road, Edinburgh EH3 9AZ 031-228 4181

HMSO's Accredited Agents

ISBN: 085311 1804